



# Clinical Persistence of *Chlamydia trachomatis* Sexually Transmitted Strains Involves Novel Mutations in the Functional $\alpha\beta\beta\alpha$ Tetramer of the Tryptophan Synthase Operon

Naraporn Somboonna,<sup>a,\*</sup> Noa Ziklo,<sup>a</sup> Thomas E. Ferrin,<sup>b</sup> Jung Hyuk Suh,<sup>a</sup> Deborah Dean<sup>a,c,d</sup>

<sup>a</sup>Center for Immunobiology and Vaccine Development, University of California San Francisco Benioff Children's Hospital Oakland Research Institute, Oakland, California, USA

<sup>b</sup>Department of Pharmaceutical Chemistry, University of California, San Francisco, California, USA

<sup>c</sup>Department of Bioengineering, University of California Berkeley and University of California San Francisco Joint Graduate Group, Berkeley and San Francisco, California, USA

<sup>d</sup>Department of Medicine and Pediatrics, University of California, San Francisco, California, USA

**ABSTRACT** Clinical persistence of *Chlamydia trachomatis* (*Ct*) sexually transmitted infections (STIs) is a major public health concern. *In vitro* persistence is known to develop through interferon gamma (IFN- $\gamma$ ) induction of indoleamine 2,3-dioxygenase (IDO), which catabolizes tryptophan, an essential amino acid for *Ct* replication. The organism can recover from persistence by synthesizing tryptophan from indole, a substrate for the enzyme tryptophan synthase. The majority of *Ct* strains, except for reference strain B/TW-5/OT, contain an operon comprised of  $\alpha$  and  $\beta$  subunits that encode TrpA and TrpB, respectively, and form a functional  $\alpha\beta\beta\alpha$  tetramer. However, *trpA* mutations in ocular *Ct* strains, which are responsible for the blinding eye disease known as trachoma, abrogate tryptophan synthesis from indole. We examined serial urogenital samples from a woman who had recurrent *Ct* infections over 4 years despite antibiotic treatment. The *Ct* isolates from each infection episode were genome sequenced and analyzed for phenotypic, structural, and functional characteristics. All isolates contained identical mutations in *trpA* and developed aberrant bodies within intracellular inclusions, visualized by transmission electron microscopy, even when supplemented with indole following IFN- $\gamma$  treatment. Each isolate displayed an altered  $\alpha\beta\beta\alpha$  structure, could not synthesize tryptophan from indole, and had significantly lower *trpBA* expression but higher intracellular tryptophan levels compared with those of reference *Ct* strain F/IC-Cal3. Our data indicate that emergent mutations in the tryptophan operon, which were previously thought to be restricted only to ocular *Ct* strains, likely resulted in *in vivo* persistence in the described patient and represents a novel host-pathogen adaptive strategy for survival.

**IMPORTANCE** *Chlamydia trachomatis* (*Ct*) is the most common sexually transmitted bacterium with more than 131 million cases occurring annually worldwide. *Ct* infections are often asymptomatic, persisting for many years despite treatment. *In vitro* recovery from persistence occurs when indole is utilized by the organism's tryptophan synthase to synthesize tryptophan, an essential amino acid for replication. Ocular but not urogenital *Ct* strains contain mutations in the synthase that abrogate tryptophan synthesis. Here, we discovered that the genomes of serial isolates from a woman with recurrent, treated *Ct* STIs over many years were identical with a novel synthase mutation. This likely allowed long-term *in vivo* persistence where active infection resumed only when tryptophan became available. Our findings indicate an emerging adaptive host-pathogen evolutionary strategy for survival in the urogenital tract that will prompt the field to further explore chlamydial persistence, evaluate

**Citation** Somboonna N, Ziklo N, Ferrin TE, Hyuk Suh J, Dean D. 2019. Clinical persistence of *Chlamydia trachomatis* sexually transmitted strains involves novel mutations in the functional  $\alpha\beta\beta\alpha$  tetramer of the tryptophan synthase operon. mBio 10:e01464-19. <https://doi.org/10.1128/mBio.01464-19>.

**Editor** Carol A. Nacy, Sequella, Inc.

**Copyright** © 2019 Somboonna et al. This is an open-access article distributed under the terms of the [Creative Commons Attribution 4.0 International license](https://creativecommons.org/licenses/by/4.0/).

Address correspondence to Deborah Dean, [ddean@chori.org](mailto:ddean@chori.org).

\* Present address: Nara Somboonna, Department of Microbiology, Faculty of Science, Chulalongkorn University, Bangkok, Thailand.

N.S. and N.Z. contributed equally to this work.

This article is a direct contribution from a Fellow of the American Academy of Microbiology. Solicited external reviewers: Ashok Aiyar, Louisiana State University School of Medicine; Margaret Hammerschlag, SUNY Downstate Medical Center.

**Received** 6 June 2019

**Accepted** 13 June 2019

**Published** 16 July 2019

the genetics of mutant *Ct* strains and fitness within the host, and their implications for disease pathogenesis.

**KEYWORDS** *Chlamydia trachomatis*, indole, interferon gamma, sexually transmitted infections, *trpA*, tryptophan synthesis

Sexually transmitted *Chlamydia trachomatis* (*Ct*) infections are highly prevalent with estimates of more than 131 million global cases occurring annually (1). They represent a major public health concern due to increasing rates worldwide and severe complications of the female reproductive tract that include tubal factor infertility, ectopic pregnancy, and chronic pelvic pain (2–4). *Ct* can also cause trachoma, a chronic ocular infection that can lead to blindness (5, 6).

Sexually transmitted infections (STIs) with *Ct* can persist for long periods of time (7–9). Most uncomplicated urogenital infections can be treated with a single dose of azithromycin with an efficacy of ~90% (10, 11). Paradoxically, treatment can also lead to a subsequent increase in the rates of urogenital infections due to interference with the development of effective immune defense against reinfection (12–14), known as the arrested immunity hypothesis (15). In *in vitro* experiments, antibiotic treatment with penicillin, rifampin, or azithromycin results in development of a persistent, nonreplicative aberrant form of the organism that can recover on removal of the antibiotic (16, 17). This may be one explanation for the recent decrease in the clinical efficacy of azithromycin (18–20).

Other factors can also cause *in vitro* persistence. In studies of human epithelial cells, interferon gamma (IFN- $\gamma$ ) induces the indoleamine 2,3-dioxygenase (IDO) enzyme that degrades tryptophan, an essential amino acid (aa) for *Ct* replication (21), and thereby inhibits *Ct* growth, forcing the organism into a persistent state. Growth resumes when tryptophan is added back to the medium (22, 23).

The genome of this obligate intracellular human pathogen has been shown to contain a tryptophan synthase operon comprised of genes encoding the tryptophan repressor (TrpR) and tryptophan synthase  $\alpha$  and  $\beta$  subunits (TrpA and TrpB, respectively) (24). Mutations in *trpA* were previously identified among trachoma strains A, Ba, and C, suggesting that this gene is involved in organotropism (25). The mutations resulted in a frameshift that was subsequently shown *in vitro* to render the enzyme nonfunctional (24, 25).

Previously, the urogenital *Ct* TrpA was found to be incapable of synthesizing indole from indole-3-glycerol phosphate (IGP) (24). However, TrpB has been shown to catalyze tryptophan production from indole, which requires a full-length TrpA protein to form a proper  $\alpha\beta\alpha$  tetramer with a tunnel for substrate binding and full synthase activity (26). Hence, only *Ct* strains with an intact operon can be rescued in *in vitro* experiments when indole is added back to the medium (25, 27, 28). However, it is conceivable that the organism could undergo selective pressure in an IFN- $\gamma$ -rich environment, such as the urogenital tract, that may promote advantageous mutations close to the active ligand-binding site of indole and/or  $\alpha$  and  $\beta$  subunit interaction sites. This could affect the structure and function of the tetramer, resulting in establishment of persistent infections *in vivo* for long-term *Ct* survival, although this has not been shown in human populations.

Here, we examined serial isolates of *Ct* urogenital F strains from a woman who had had recurrent *Ct* STIs over a number of years despite antibiotic treatment. Our data indicate that mutations in the tryptophan synthase operon of these urogenital strains altered tetramer function and likely resulted in the *in vivo* persistence of the isolate in the patient described, indicating a selective adaptive host-pathogen evolutionary strategy for survival.

## RESULTS

***C. trachomatis* clinical F strains I to IV contain a frameshift deletion mutation causing *trpA* elongation and cluster as a phylogenetic subbranch of urogenital strains.** Clinical strains were isolated from a female who had recurring infections over

a period of 4 years denoted F I to IV (F I-IV). The four strains had identical genomes (GenBank accession no. SRA051574.1 [29]), suggesting persistent infection with the same strain. *ompA*, a standard gene used for *Ct* genotyping, differed by a single nucleotide polymorphism (SNP) from reference strain F/IC-Cal3, encoding a synonymous aa mutation. *trpR* and *trpB* sequences were identical to those of the reference strain (Fig. 1A and B); *trpA* sequences contained a deletion at nucleotide (nt) 758, compared with F/IC-Cal3, causing a nonsynonymous aa mutation, G253D, and elongation of TrpA by two aas (254N 255L) (Fig. 1C). These data were compared to the 20 known *Ct* reference strains, and none had this mutation.

Of seven novel San Francisco clinical F strains, F/SF10 was identical to D/UW3 and K/UW31 at the N terminus and to E/Bour at the C terminus (Fig. 1C). F/SF14 was similar to E/Bour, while F/SF21 was identical to K/UW31 and D/UW3 (Fig. 1C). Of the 59 publicly available F sequences, F/HonMPB36 shared an identical *trpA* sequence with F/NL38 and F/S4410, while *trpR* was truncated after 90 bp (Fig. 1A to C).

*trpA* phylogeny clustered F I-IV as a subbranch of F/IC-Cal3 (Fig. 2). The tree differentiated ocular trachoma strains (A, Ba, C, and Da) from noninvasive urogenital (D-K) and invasive lymphogranuloma venereum (L<sub>1</sub>-L<sub>3</sub>) strains, which is similar to previous phylogenetic analyses of this gene. TrpA phylogeny was similar to *trpA* (see Fig. S1 in the supplemental material).

**Comparative structure analyses of TrpB and TrpA for clinical strains F I-IV reveals mutations within the functional  $\alpha\beta\beta\alpha$  tetrad complex.** F I-IV TrpA was elongated by two aas, 254N and 255L, to a total of 255 aas. Since there are no crystal structures of the *Ct* tryptophan operon proteins, we used MODELLER (30) to model the  $\alpha$  and  $\beta$  subunits based on homologies to known crystal structure templates. The TrpA structure (Fig. 3A, cyan) had >95% correct folds and a GA341 MODELLER score of 1.0, indicating a highly reliable modeling structure (31), and aligned well with templates last bacterial common ancestor (LBCA) 5ey5 (32), which had the highest identity to the clinical F TrpA of 31.76% (Fig. 3A, magenta), *Mycobacterium tuberculosis* 5tch (28.63% identity), and *Salmonella enterica* serotype Typhimurium 1qop (25.1% identity). The elongation was located at the end of the protein (Fig. 3A and B, yellow surface of ribbons), rather than at the active site. F/IC-Cal3 TrpA, which is known to be functional, had good homology to the 5ey5 structure (32.02% identity) (Fig. 3C and D, yellow), while A/HAR13 had 34.43% similarity for the 183 aas but only 23.07% similarity to the entire 5ey5 protein (Fig. 3E and F; green).

Dimer subunits  $\alpha$  and  $\beta$  have either an open or closed conformation. Closing of the  $\alpha$  subunit is associated with  $\alpha$ -loop L6 ( $\alpha$ -L6) mobility that requires residues  $\alpha$ 176 to  $\alpha$ 196 (Fig. 3B and D), which, together with the  $\beta$ -COMM domain (Fig. 4A to C, bold black), are critical for the closed conformation and formation of the tunnel that traps indole (33). A/HAR13 has a predicted three-dimensional (3D) model that does not have a complete  $\alpha$ -L6 (Fig. 3E and F, green) due to truncation at residue 183 in proximity to the  $\beta$ -COMM domain (Fig. 4C, black) and no proximal alpha helix (Fig. 3F, arrow). Dimers for clinical F and F/IC-Cal3 had almost identical sequences and exhibited comparable structures with >95% correct folds (Fig. 4A and B) and a GA341 MODELLER score of 1.0.

The TrpA aa alignment of F/IC-Cal3, A/HAR13, and F I-IV along with templates 5ey5, 5tch, and 1qop are shown in Fig. 5A. Highlighted in magenta are residues located around the tunnel comprised of Phe<sup>22</sup>, Glu<sup>49</sup>, Asp<sup>60</sup>, Thr<sup>183</sup>, Gly<sup>211</sup>, Gly<sup>213</sup>, Gly<sup>234</sup>, and Ser<sup>235</sup> that are based on the 1qop sequence.  $\alpha$ -L6 residues  $\alpha$ 176-196 are in cyan. The clinical F mutation at  $\alpha$ 253 is highlighted in green, and protein elongation in yellow. Figure 5B shows the TrpA phylogenetic tree.

**Recoverable infectivity of *C. trachomatis* clinical strains F I-IV was significantly lower than for F/IC-Cal3 following tryptophan starvation and rescue.** To assess whether F I-IV can synthesize tryptophan from indole despite mutations in the  $\alpha$  subunits of the tryptophan operon, *in vitro* tryptophan starvation and indole rescue assays were performed, comparing F I-IV and F/IC-Cal3 (see Materials and Methods). F I-IV were not able to recover from tryptophan starvation using indole (Fig. 6A) at 48 h

**A**

```

31 88 106 166 244 271 285
A/Har-13 GCT...TCG.AGCCGAA...CTC...TTA.CAA.TGA
Ba/Apache-2 GCT...TCG.AGCCGAA...CTC...TTA.CAA.TGA
C/TW-3 GCT...TCG.AGCCGAA...CTC...TTA.CAA.TGA
Da/TW-448 GCT...TCG.AGCCGAA...CTC...TTA.CAA.TGA
D/UW-3 GCT...TCG.AGCCGAA...CTC...TTA.CAA.TGA
E/Bour GCT...TCG.AGCCGAA...CTC...TTA.CAA.TGA
F/IC-Cal3 GCT...TCG.AGCCGAA...CTC...TTA.CAA.TGA
F/I GCT...TCG.AGCCGAA...CTC...TTA.CAA.TGA
F/II GCT...TCG.AGCCGAA...CTC...TTA.CAA.TGA
F/III GCT...TCG.AGCCGAA...CTC...TTA.CAA.TGA
F/IV GCT...TCG.AGCCGAA...CTC...TTA.CAA.TGA
F/S4410 GCT...TCG.AGCCGAA...CTC...TTA.CAA.TGA
F/NL38 GCT...TCG.AGCCGAA...CTC...TTA.CAA.TGA
F/STN110 GCT...TCG.AGCCGAA...CTC...TTA.CAA.TGA
F/SF10 GCT...TCG.AGCCGAA...CTC...TTA.CAA.TGA
F/SF21 GCT...TCG.AGCCGAA...CTC...TTA.CAA.TGA
F/Fin213 GCT...TCG.AGCCGAA...CTC...TTA.CAA.TGA
F/Fin219 GCT...TCG.AGCCGAA...CTC...TTA.CAA.TGA
G/UW-524 GCT...TCG.AGCCGAA...CTC...TTA.CAA.TGA
H/UW-4 GCT...TCG.AGCCGAA...CTC...TTA.CAA.TGA
I/UW-12 GCT...TCG.AGCCGAA...CTC...TTA.CAA.TGA
Ia/IU-4168 GCT...TCG.AGCCGAA...CTC...TTA.CAA.TGA
J/UW-36 GCT...TCG.AGCCGAA...CTC...TTA.CAA.TGA
Ja/UW-92 GCT...TCG.AGCCGAA...CTC...TTA.CAA.TGA
K/UW-31 GCT...TCG.AGCCGAA...CTC...TTA.CAA.TGA
L3/404 GCT...TCG.AGCCGAA...CTC...TTA.CAA.TGA
A S S E L L Q .
31 88 106 166 244 271 285
L1/440 GCT...TCG.AGCCGAA...CTC...TTA.CCA.TGA
A S S E L L P .
L2/434 GCT...TCG.GCCGAA...CTC.TCA.CAA.TGA
L2a/TW-396 GCT...TCG.GCCGAA...CTC.TCA.CAA.TGA
L2b/UCH GCT...TCG.GCCGAA...CTC.TCA.CAA.TGA
L2c GCT...TCG.GCCGAA...CTC.TCA.CAA.TGA
A S G E L S Q .
F/SF14 GCT...TCG.GCCGAA...TTC...TTA.CAA.TGA
A S G E F L Q .
F/SwabB8 ACT...TCG.AGCCGAA...CTC...TTA.CAA.TGA
T S S E L L Q .
31 90
F/HonMPB36 GCT...TAG
A -
    
```

**B**

```

55 106 178 205 505 694 859 1015 1141 1179
A/Har-13 GCC.AGT..AGT..AGA.CAA.TCC.GAC.AAC..CCA.TAA
C/TW-3 GCC.AGT..AGT..AGA.CAA.TCC.GAC.AAC..CCA.TAA
A S S R Q S D N P .
Ba/Apache-2 GCC.AGT..AAT..AGA.CAA.TCC.GAC.AAC..TCA.TAA
A S N R Q S D N S .
D/UW-3 GCC.AGT..AAT..AGA.CAA.TCC.GAC.AAC..CCA.TAA
Da/TW-448 GCC.AGT..AAT..AGA.CAA.TCC.GAC.AAC..CCA.TAA
E/Bour GCC.AGT..AAT..AGA.CAA.TCC.GAC.AAC..CCA.TAA
F/IC-Cal3 GCC.AGT..AAT..AGA.CAA.TCC.GAC.AAC..CCA.TAA
F/I GCC.AGT..AAT..AGA.CAA.TCC.GAC.AAC..CCA.TAA
F/II GCC.AGT..AAT..AGA.CAA.TCC.GAC.AAC..CCA.TAA
F/III GCC.AGT..AAT..AGA.CAA.TCC.GAC.AAC..CCA.TAA
F/IV GCC.AGT..AAT..AGA.CAA.TCC.GAC.AAC..CCA.TAA
F/SF10 GCC.AGT..AAT..AGA.CAA.TCC.GAC.AAC..CCA.TAA
F/SF21 GCC.AGT..AAT..AGA.CAA.TCC.GAC.AAC..CCA.TAA
F/SwabB8 GCC.AGT..AAT..AGA.CAA.TCC.GAC.AAC..CCA.TAA
F/HonMPB36 GCC.AGT..AAT..AGA.CAA.TCC.GAC.AAC..CCA.TAA
F/Fin213 GCC.AGT..AAT..AGA.CAA.TCC.GAC.AAC..CCA.TAA
F/Fin219 GCC.AGT..AAT..AGA.CAA.TCC.GAC.AAC..CCA.TAA
G/UW-524 GCC.AGT..AAT..AGA.CAA.TCC.GAC.AAC..CCA.TAA
I/UW-12 GCC.AGT..AAT..AGA.CAA.TCC.GAC.AAC..CCA.TAA
K/UW-31 GCC.AGT..AAT..AGA.CAA.TCC.GAC.AAC..CCA.TAA
A S N R Q S D N P .
55 106 178 205 505 694 859 1015 1141 1179
F/STN110 GCC.AGT..AAT..AGA.CAA.TCC.AAC.AAC..CCA.TAA
A S N R Q S N N P .
Ia/IU-4168 GCC.AAT..AAT..AAA.CAA.TCC.GAC.AAC..CCA.TAA
A N N K Q S D N P .
H/UW-4 GCC.AAT..AAT..AAA.CAA.TCC.GAC.AAT..CCA.TAA
J/UW-36 GCC.AAT..AAT..AAA.CAA.TCC.GAC.AAT..CCA.TAA
Ja/UW-92 GCC.AAT..AAT..AAA.CAA.TCC.GAC.AAT..CCA.TAA
L3/404 GCC.AAT..AAT..AAA.CAA.TCC.GAC.AAT..CCA.TAA
L1/440 GCC.AAT..AAT..AAA.CAA.TCC.S D N P .
A N N K Q S D N P .
F/S4410 ACC.AGT..AAT..AAA.AAA.TCC.GAC.AAC..CCA.TAA
F/NL38 ACC.AGT..AAT..AAA.AAA.TCC.GAC.AAC..CCA.TAA
F/SF14 ACC.AGT..AAT..AAA.AAA.TCC.GAC.AAC..CCA.TAA
T S N K K S D N P .
L2/434 GCC.AGT..AAT..AGA.CAA.TTC.GAC.AAT..CCA.TAA
A S N R Q F D N P .
L2a/TW-396 GCC.AGT..AAT..AGA.CAA.TCC.GAC.AAT..CCA.TAA
L2b/UCH GCC.AGT..AAT..AGA.CAA.TCC.GAC.AAT..CCA.TAA
L2c GCC.AGT..AAT..AGA.CAA.TCC.GAC.AAT..CCA.TAA
A S N R Q S D N P .
    
```

**C**

```

37 109 118 310 343 364 406 496 502 508 526 552
A/Har-13 CCA..CAA..GTC.AGG..GCG..GTT..CC---TTTT..CAC..GCA..CTT..TA-CAAG..TAG
Ba/Apache-2 CCA..CAA..GTC.AGG..GCG..GTT..CC---TTTT..CAC..GCA..CTT..TA-CAAG..TAG
C/TW-3 CCA..CAA..GTC.AGG..GCG..GTT..CC---TTTT..CAC..GCA..CTT..TA-CAAG..TAG
Da/TW-448 CCA..CAA..GTC.AGG..GCG..GTT..CC---TTTT..CAC..GCA..CTT..TA-CAAG..TAG
P Q V R A V H A L Y K .
37 109 118 310 343 364 406 499 502 511 529 554 643 762
D/UW-3 CTA..CAA..GTC.AGG..GCG..GTT..CCATTTTTT..TAC..GCA..TTT..TGTCAA..TAG..GCA..GGATAA
F/SF21 CTA..CAA..GTC.AGG..GCG..GTT..CCATTTTTT..TAC..GCA..TTT..TGTCAA..TAG..GCA..GGATAA
K/UW-31 CTA..CAA..GTC.AGG..GCG..GTT..CCATTTTTT..TAC..GCA..TTT..TGTCAA..TAG..GCA..GGATAA
L Q V R A V F Y A F C Q A G .
F/SF10 CTA..CAA..GTC.AGG..GCG..GTT..CCATTTTTT..TAC..GCA..TTT..TATCAA..TAG..GCA..GGATAA
L Q V R A V F Y A F Y Q A G .
E/Bour CCA..CAA..GTC.AGG..GCG..GTT..CCATTTTTT..TAC..GCA..TTT..TGTCAA..TAG..GCA..GGATAA
F/SF14 CCA..CAA..GTC.AGG..GCG..GTT..CCATTTTTT..TAC..GCA..TTT..TGTCAA..TAG..GCA..GGATAA
P Q V R A V F Y A F C Q A G .
F/Fin213 CCA..CAA..GTC.AGG..GCG..GTT..CCATTTTTT..TAC..ACA..TTT..TATCAA..TAG..GCA..GGATAA
P Q V R A V F Y T F Y Q A G .
F/Fin219 CCA..CAA..GTC.AGG..GCG..GTT..CCATTTTTT..TAC..GCA..TTT..TATCAA..TAG..GTA..GGATAA
P Q V R A V F Y A F Y Q V G .
F/IC-Cal3 CCA..CAA..GTC.AGG..GCG..GTT..CCATTTTTT..TAC..GCA..TTT..TATCAA..TAG..GCA..GGATAA
F/SwabB8 CCA..CAA..GTC.AGG..GCG..GTT..CCATTTTTT..TAC..GCA..TTT..TATCAA..TAG..GCA..GGATAA
F/STN110 CCA..CAA..GTC.AGG..GCG..GTT..CCATTTTTT..TAC..GCA..TTT..TATCAA..TAG..GCA..GGATAA
G/UW-524 CCA..CAA..GTC.AGG..GCG..GTT..CCATTTTTT..TAC..GCA..TTT..TATCAA..TAG..GCA..GGATAA
I/UW-12 CCA..CAA..GTC.AGG..GCG..GTT..CCATTTTTT..TAC..GCA..TTT..TATCAA..TAG..GCA..GGATAA
P Q V R A V F Y A F Y Q A G .
H/UW-4 CCA..CGA..GTC.AGG..GTG..GTT..CCATTTTTT..TAC..GCA..TTT..TATCAA..TAG..GCA..GGATAA
Ia/IU-4168 CCA..CGA..GTC.AGG..GTG..GTT..CCATTTTTT..TAC..GCA..TTT..TATCAA..TAG..GCA..GGATAA
J/UW-36 CCA..CGA..GTC.AGG..GTG..GTT..CCATTTTTT..TAC..GCA..TTT..TATCAA..TAG..GCA..GGATAA
Ja/UW-92 CCA..CGA..GTC.AGG..GTG..GTT..CCATTTTTT..TAC..GCA..TTT..TATCAA..TAG..GCA..GGATAA
P R V R V V F Y A F Y Q A G .
L3/404 CCA..CGA..GTC.AGG..GTG..GTT..CCATTTTTT..TAC..GCA..TTT..TATCAA..TAG..GCA..GGATAA
L1/440 CCA..CGA..GTC.AGG..GTG..GTT..CCATTTTTT..TAC..GCA..TTT..TATCAA..TAG..GCA..GGATAA
P R V R V V F Y A F Y E A G .
L2/434 CCA..CGA..GTT..AGG..GCG..GTT..CCATTTTTT..TAC..GCA..TTT..TATGAA..TAG..GCA..GGATAA
L2a/TW-396 CCA..CGA..GTT..AGG..GCG..GTT..CCATTTTTT..TAC..GCA..TTT..TATGAA..TAG..GCA..GGATAA
L2b/UCH CCA..CGA..GTT..AGG..GCG..GTT..CCATTTTTT..TAC..GCA..TTT..TATGAA..TAG..GCA..GGATAA
L2c CCA..CGA..GTT..AGG..GCG..GTT..CCATTTTTT..TAC..GCA..TTT..TATGAA..TAG..GCA..GGATAA
P R V R A V F Y A F Y E A G .
37 109 118 310 343 364 406 499 502 511 529 554 643 762
F/S4410 CCA..CAA..GTC.AGT..GCG..ATT..CCATTTTTT..TAC..GCA..TTT..TATCAA..TAG..GCA..GGATAA
F/NL38 CCA..CAA..GTC.AGT..GCG..ATT..CCATTTTTT..TAC..GCA..TTT..TATCAA..TAG..GCA..GGATAA
F/HonMPB36 CCA..CAA..GTC.AGT..GCG..ATT..CCATTTTTT..TAC..GCA..TTT..TATCAA..TAG..GCA..GGATAA
P Q V S A I F Y A F Y Q A G .
37 109 118 310 343 364 406 499 502 511 529 554 643 761 768
F/I CCA..CAA..GTC.AGG..GCG..GTT..CCATTTTTT..TAC..GCA..TTT..TATCAA..TAG..GCA..G-ATAATTATGA
F/II CCA..CAA..GTC.AGG..GCG..GTT..CCATTTTTT..TAC..GCA..TTT..TATCAA..TAG..GCA..G-ATAATTATGA
F/III CCA..CAA..GTC.AGG..GCG..GTT..CCATTTTTT..TAC..GCA..TTT..TATCAA..TAG..GCA..G-ATAATTATGA
F/IV CCA..CAA..GTC.AGG..GCG..GTT..CCATTTTTT..TAC..GCA..TTT..TATCAA..TAG..GCA..G-ATAATTATGA
P Q V R A V F Y A F Y Q A D N L -
    
```

**FIG 1** *C. trachomatis* clinical strains F I to IV (F I-IV) contain a *trpA* frameshift causing TrpA elongation. (A to C) Partial nucleotide sequences showing *trpR* (A), *trpB* (B), and *trpA* (C) polymorphisms of the four serial (Continued on next page)

postinfection (hpi); these strains (+IFN- $\gamma$  -Trp +indole) had significantly fewer inclusion-forming units per milliliter (IFUs/ml) compared to the same strains receiving media without IFN- $\gamma$  (-IFN- $\gamma$ ) ( $P < 0.01$ ). Furthermore, when tryptophan was added (-IFN- $\gamma$  -Trp +Trp), recoverable IFUs/ml were significantly higher than the starved strains supplemented with indole (+IFN- $\gamma$  -Trp +indole) ( $P < 0.05$ ). F/IC-Cal3 had an overall higher growth rate in comparison to F I-IV for every condition ( $P < 0.05$ ). The addition of indole to the tryptophan-depleted media (+IFN- $\gamma$  -Trp +indole) was sufficient to yield significantly higher IFUs/ml compared to IFN- $\gamma$ -treated F/IC-Cal3 (+IFN- $\gamma$ ) ( $P < 0.01$ ).

To further evaluate the lack of recovery for F I-IV, inclusion morphology was examined under IFN- $\gamma$  and indole treatment (+IFN- $\gamma$  -Trp +Indole) at 48 hpi. Clinical F strain inclusions were considerably smaller (~100 to 200  $\mu\text{m}^2$ ; Fig. 6C) than those formed by F/IC-Cal3 (~500 to 600  $\mu\text{m}^2$ ; Fig. 6B). In addition, under the same treatment conditions, transmission electron microscopy (TEM) images showed that clinical strain F II contained inclusion bodies with numerous aberrant bodies compared with F/IC-Cal3 at 48 hpi (Fig. 6D and E). The morphology and TEM findings were similar for F I, III, and IV (data not shown).

***trpBA* mRNA expression for clinical strains F I-IV was significantly reduced compared to F/IC-Cal3 under tryptophan depletion and rescue.** To verify F/IC-Cal3 tryptophan operon activity compared to F I-IV, *trpBA* mRNA expression levels were measured at 24 and 48 hpi under the conditions of tryptophan starvation and rescue with either indole or tryptophan (Fig. 7). At 24 hpi, during tryptophan starvation (-Trp) and rescue with indole (-Trp +Indole) or tryptophan (-Trp +Trp), F/IC-Cal3 had significantly higher expression levels of *trpBA* compared to F I-IV (Fig. 7). Additionally, there was a trend in upregulation of F/IC-Cal3 *trpBA* expression when incubated in tryptophan-depleted media (-Trp) compared with indole (-Trp +Indole;  $P = 0.0909$ ) and tryptophan supplementation (-Trp +Trp;  $P = 0.0736$ ), indicating activity of the tetrad during tryptophan starvation. *trpBA* levels were also measured at 12, 36, and 60 hpi; F/IC-Cal3 levels were upregulated starting at 12 hpi, whereas F I-IV *trpBA* levels were relatively similar throughout development with 4.33-, 2.25-, and 3.16-fold lower levels than F/IC-Cal3, respectively (data not shown). *trpR* expression levels showed a similar trend, in which indole supplementation after tryptophan starvation was not sufficient to downregulate *trpR* in clinical F strain (data not shown).

***In vitro* intracellular tryptophan concentrations vary significantly for reference strain F/IC-Cal3 compared with clinical strains F I-IV.** To determine whether F I-IV can synthesize and utilize tryptophan following tryptophan starvation and indole or tryptophan rescue, intracellular tryptophan concentrations were measured and compared to those of F/IC-Cal3 (Fig. 8A and B). Using IFN- $\gamma$  to deplete tryptophan, F I-IV had significantly higher intracellular tryptophan concentrations than those of F/IC-Cal3 ( $P < 0.0001$ ; Fig. 8B) with a trend for tryptophan-depleted media ( $P = 0.0559$ ; Fig. 8A). When tryptophan-depleted cultures were supplemented with indole, intracellular tryptophan concentrations were significantly higher for F I-IV than for F/IC-Cal3 (Fig. 8A,  $P < 0.05$ ; Fig. 8B,  $P < 0.0001$ ). These findings were supported by the higher levels of intracellular tryptophan concentrations when tryptophan-depleted F I-IV cultures were

#### FIG 1 Legend (Continued)

clinical strains F I-IV compared to 20 *C. trachomatis* (Ct) reference strains (A/HAR13, Ba/Apache2, C/TW3, D/UW3, Da/TW448, E/Bour, F/ICCal3, G/UW57, H/UW4, I/UW12, Ia/IU4168, J/UW36, Ja/UW92, K/UW31, L1/440, L<sub>2</sub>/434, L<sub>2</sub>a/TW396, L<sub>2</sub>b/UCH-1/proctitis, L<sub>2</sub>c, and L<sub>3</sub>/404) including novel clinical F strains from the San Francisco Bay Area ( $n = 7$ ) and all F strains previously sequenced and available from public databases ( $n = 59$ ). A period in the sequence denotes homologous sequences that are not shown. Dashes denote nucleotide deletions at positions A408, T409, T410, and T528 for *trpA* of ocular strains and at position 758 for *trpA* of clinical strains F I-IV. Bold nucleotide letters denote substitution mutations, while bold amino acid letters denote nonsynonymous amino acid substitutions. Strains with homologous sequences are not shown: F/SotonF1-F4, F/Soton18-137, F/R4663-28312, F/STN15-22, F/UK35155-770010, F/SW4-5, F/SWFP, F/S1470-3948, F/NI1, F/NL30-36, F/Aus20, F/C55, F/It686-688, F/Sou9-100, F/Swab5, F/SwabB5, F/Fin106-219, and F/SF7-19. These strains had genes that were similar to the *trpR* gene of A/HAR13-L3/404, the *trpB* gene of D/UW-3-K/UW-31, and the *trpA* gene of F/IC-Cal3-I/UW-12.

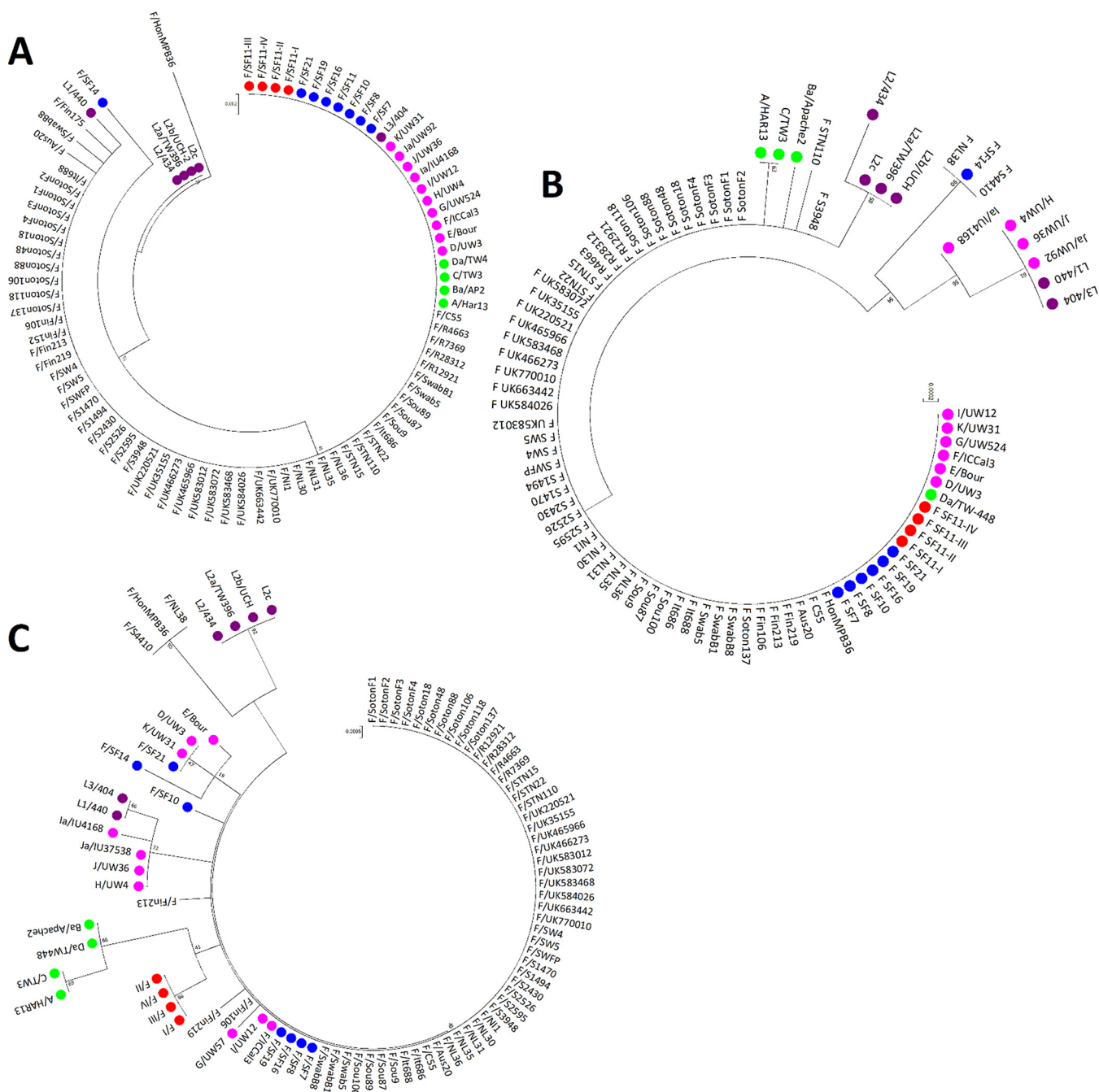


**FIG 2** Phylogeny of *trpRBA* for 20 *Ct* reference strains, clinical F I-IV strains and other publicly available *C. trachomatis* F strains clustered F I-IV as a subbranch of reference strain F/IC-Cal3. (A to C) *trpR* (A), *trpB* (B), and *trpA* (C) maximum likelihood trees were constructed using Tamura-3-parameters method with 10,000 bootstrap replicates of the F I-IV strains, seven novel clinical F strains collected from San Francisco Bay Area clinics, 59 *Ct* clinical F strains available from public databases, and the 20 reference strains of *Ct*. B/UW-3 contained no *trpRBA* operon and therefore was not included. Scale bar at the top and at each branch length correspond to sequence divergence scale and time. The numbers at branches indicate bootstrap score. Red dots, F I-IV strains; blue dots, San Francisco F strains; magenta dots, reference *Ct* strains; green dots, ocular *Ct* strains; maroon dots, LGV strains.

supplemented with tryptophan compared to F/IC-Cal3 (Fig. 8A,  $P < 0.01$ ; Fig. 8B,  $P < 0.0001$ ).

**DISCUSSION**

As an obligate intracellular bacterium and tryptophan auxotroph, *Ct* relies on host tryptophan pools to replicate. However, despite the fact that *Ct* has a long history of reductive evolution and loss of key functional enzymes (34), the organism has, by and

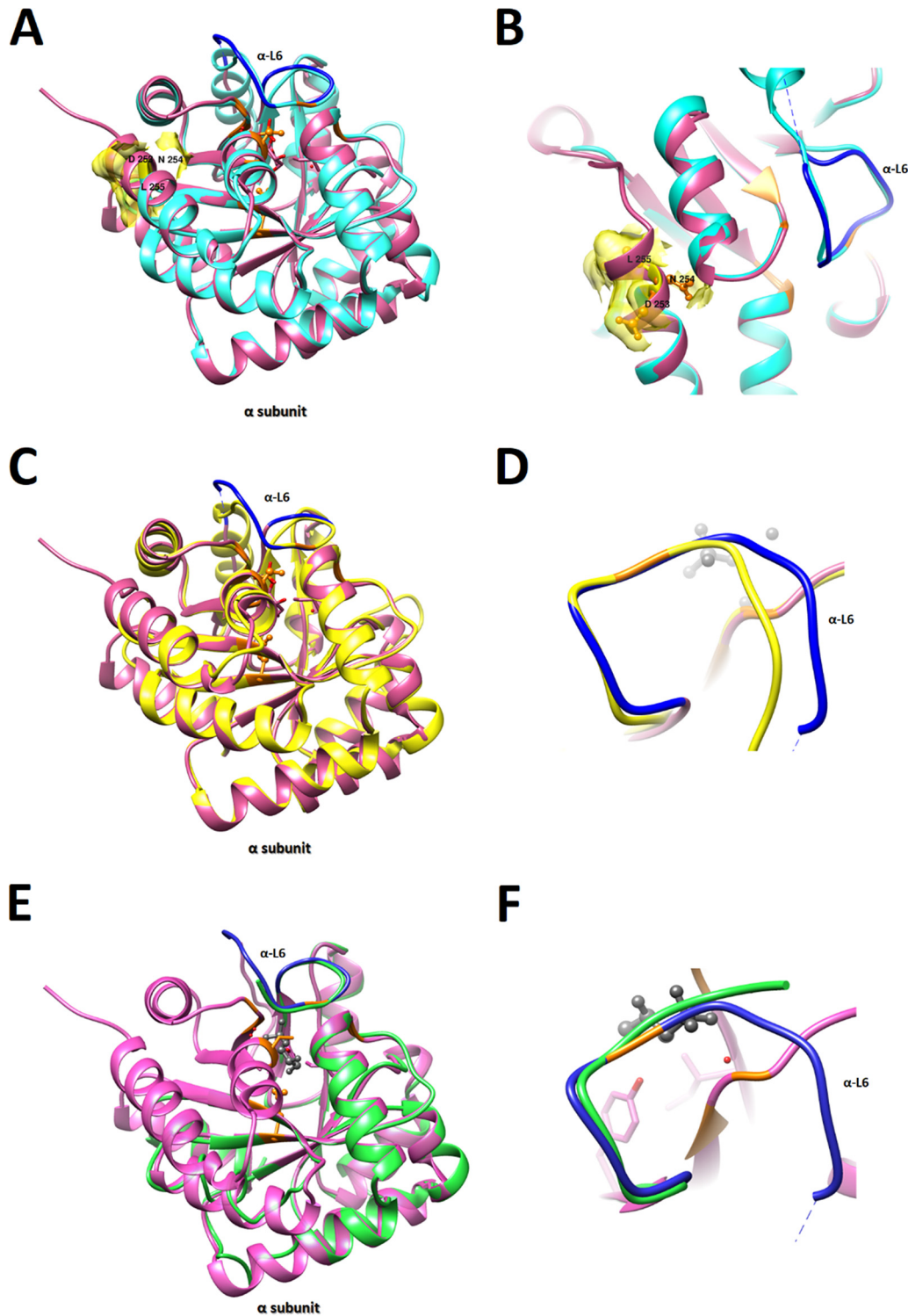


**FIG 3** TrpA 3D predicted structures of clinical and reference *C. trachomatis* strains. (A to F) TrpA structures of *Ct* clinical strains F I-IV (cyan) (A), elongation of clinical strain F  $\alpha$ 254N and  $\alpha$ 255L aa surface area (yellow) and  $\alpha$ -loop L6 ( $\alpha$ -L6) of template 5tch (blue) and clinical strain F (cyan) (B), *Ct* urogenital reference strain F/IC-Cal3 (yellow) (C),  $\alpha$ -L6 of template 5tch (blue) and F/IC-Cal3 (yellow) (D), *Ct* ocular reference strain A/HAR13 (green) (E), and  $\alpha$ -L6 of template 5tch (blue) and A/HAR13 (green, truncated) (F). All structures were constructed using the template from the published crystal structures of the reconstructed putative last bacterial common ancestor (LBCA) tryptophan synthase 5ey5 (magenta) using MOD-ELLER with visualization construction using Chimera (see Materials and Methods). Residues involved in both catalytic and subunit interaction are shown in orange. Dashed lines represent the tunnel and substrate binding site at the  $\alpha$  subunit.

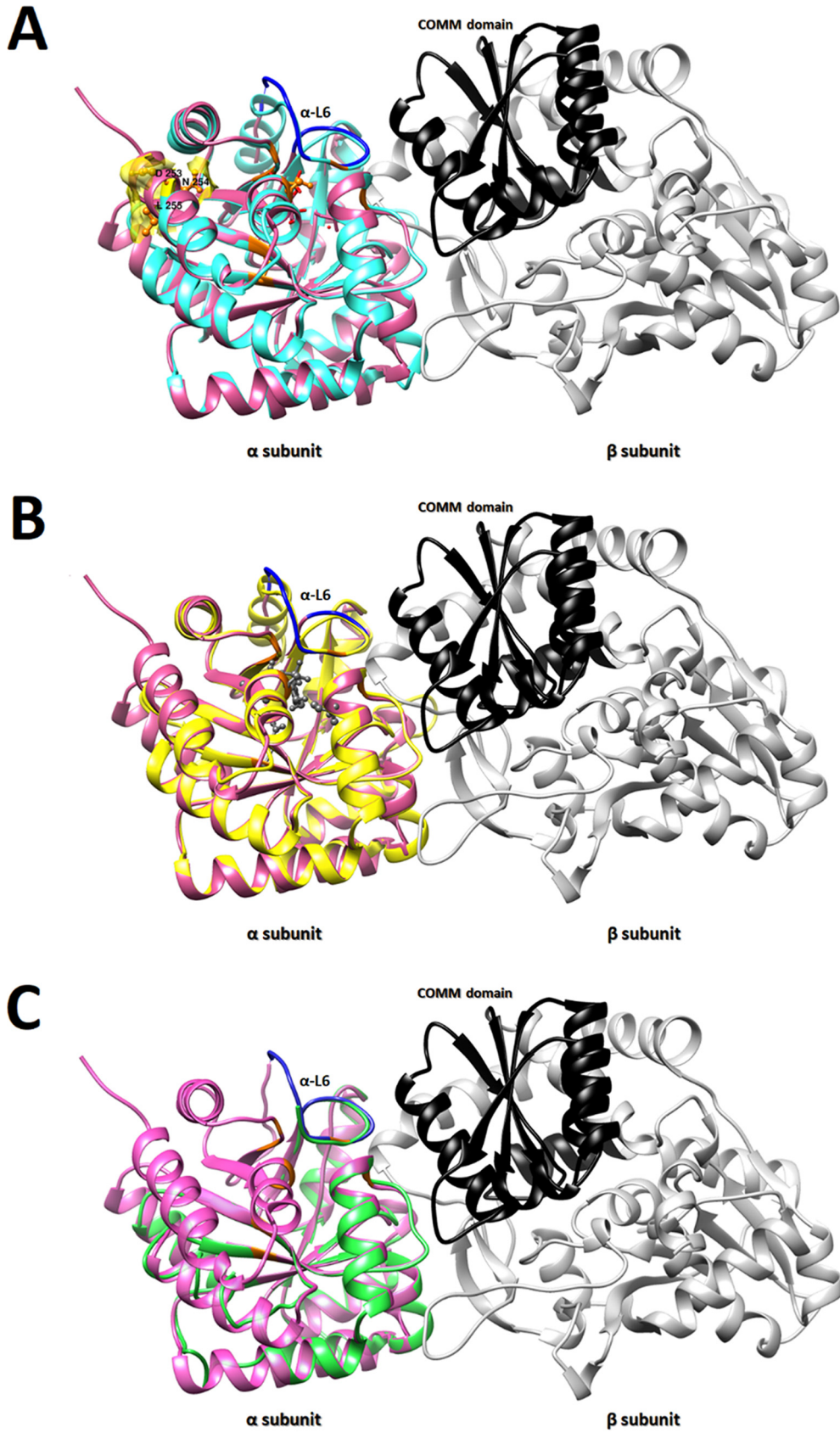


**FIG 4** Comparative structure analyses of TrpB and TrpA for clinical strains F I-IV reveals mutations within the functional  $\alpha\beta\beta\alpha$  tetrad complex. (A to C) TrpA-TrpB dimer structures of *Ct* clinical strain F (cyan) (A), *Ct* urogenital (Continued on next page)

large, retained the tryptophan synthase operon. Previous *in vitro* studies have shown that tryptophan depletion can drive *Ct* into a persistent form, yet with the addition of indole or indole-producing bacteria to the media, urogenital but not ocular strains have been able to synthesize tryptophan and complete their developmental cycle (25, 28).

Comparative genomics of *Ct* strains from different lineages have shown that the ocular strains emerged from the urogenital strains around 10 to 15 million years ago (29). Through subsequent reductive evolution, ocular strains lost their ability to synthesize tryptophan. The low prevalence or lack of indole-producing bacteria in the conjunctiva (35, 36) may have contributed to this loss. However, some indole producers such as *Propionibacterium acnes* and *Escherichia coli* have routinely been found in the microbiota of healthy conjunctiva (37). Others have proposed that ocular strains lost their functional operon to maximize fitness (36). During infection and upregulation of IFN- $\gamma$ , *Ct trpBA* expression is induced, but in the absence of indole, the  $\beta$  subunit catalyzes the deamination of L-serine to produce pyruvate and ammonia (38), an antimicrobial agent that can also induce apoptosis of epithelial cells, especially under higher pH levels (39), similar to those found on the ocular surface of healthy patients (40). Losing tetramer function would prevent the production of this deleterious agent and promote *Ct* growth. Sherchand and Aiyar recently demonstrated that indole derivatives, produced by some gut bacteria and present in serum, can induce the expression of *Ct trpBA*, despite sufficient tryptophan concentrations (41). They found that these indole derivatives act as a derepressor of *Ct TrpR*, and during infection, when indole is absent from the media, the ammonia produced by a functional tryptophan synthase enzyme has bactericidal effects on *Ct* growth. This effect was absent when ocular *Ct* strain A2497 or a urogenital D *trpB*-null strain with a point mutation in *TrpB* was used (41).

In this study, we identified an F strain that was repeatedly isolated from the endocervix of a woman with asymptomatic *Ct* infections. The F I-IV genomes were 100% identical, suggesting a persistent infection that was able to survive in spite of the host immune response and repeated antibiotic treatment. The strains had a unique  $\alpha$  subunit point mutation that caused a frameshift and elongation of the *TrpA* by two aas unlike any publicly available F strains. This is the first study to document a novel urogenital *Ct* mutation in *trpA* with an *in vivo* advantage for a nonfunctional operon in a clinical setting.

The clinical F *TrpA* 3D protein model showed that  $\alpha$ 254N and  $\alpha$ 255L at the C terminus were not precisely located at the active ligand-binding site of indole. However, the G253D mutation replaced the nonpolar glycine with the acidic, negatively charged aspartic acid near the active  $\alpha$  subunit site and the 25-Å-long tunnel that connects both subunits (Fig. 3B; dashed black line). Since the C-terminal residues for the LBCA Sey5, *M. tuberculosis* Stch, and *S. Typhimurium* 1qop are basic, the surface polarity change could alter the structural position and folding of residues in the tunnel (42, 43) with functional consequences for the clinical F tryptophan synthase. Furthermore, while the *Ct TrpA* cannot capture IGP to initiate indole production and does not produce indole, indole is captured by the  $\alpha$  subunit, and in other bacterial species, the tunnel has been shown to accommodate indole channeling from the  $\alpha$  subunit to the  $\beta$  subunit (44).

The stability of the closed conformation depends on the  $\alpha$  subunit movement of  $\alpha$ -L6 and the allosteric connection between the  $\alpha$  subunit glycine residue (Gly $\alpha$ 181) and the  $\beta$  subunit serine residue (Ser $\beta$ 178) (45). Interestingly, none of the *Ct* strains had serine in this position; clinical F and F/IC-Cal3 had alanine, while A/HAR13 had leucine

#### FIG 4 Legend (Continued)

reference strain F/IC-Cal3 (yellow) (B), and *Ct* ocular reference strain A/HAR13 (green) (C). The *TrpB* structure is shown with the  $\beta$ -COMM domain in black. All *TrpA* and *TrpB* structures were constructed using the template from the published crystal structures of the reconstructed putative last bacterial common ancestor (LBCA) tryptophan synthase Sey5 (magenta) using MODELLER with visualization construction using Chimera (see Materials and Methods).  $\alpha$ -L6 residues are shown in blue, and residues involved in both catalytic and subunit interaction are shown in orange.

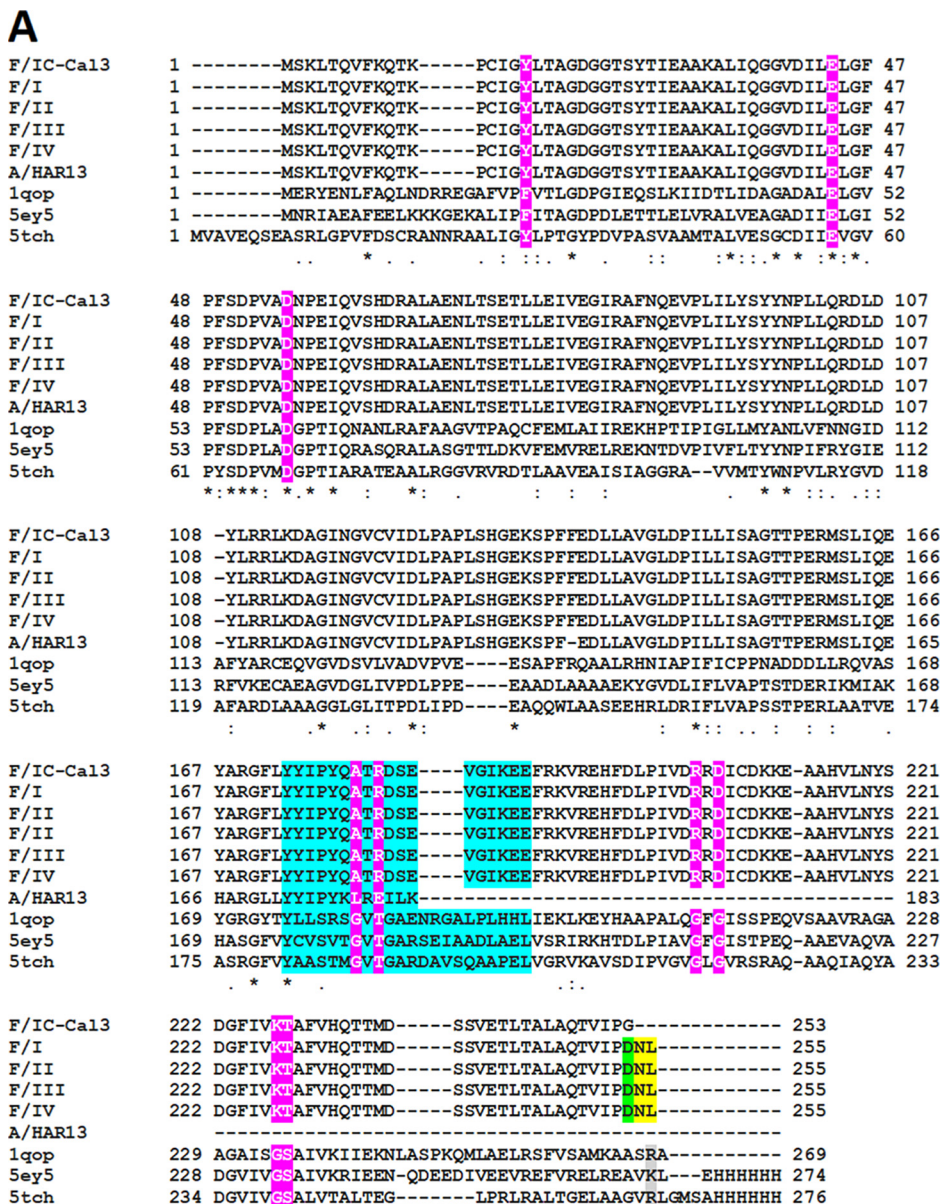


**FIG 5** TrpA amino acid alignment and phylogeny of *C. trachomatis* clinical strains F I-IV, A/HAR13, F/IC-Cal3, and Protein Data Bank (PDB) templates. (A) For 3D model reconstructions, amino acid alignments of *Ct* clinical (Continued on next page)

(Fig. 5A). This suggests that *Ct* tetramer function may be somewhat compromised, even for strains with the complete sequence like F/IC-Cal3, and thus inefficient at producing tryptophan. The A/HAR13 *TrpA* model revealed a truncated protein in the middle of  $\alpha$ -L6, explaining the inability of this strain and other truncated strains to form a closed conformational state to capture indole. The allosteric effect between the two subunits is essential to the efficiency of the enzyme and is different among various bacteria. *Ct* *TrpB* was found to be inactive in the absence of a full-length *TrpA* (24). In *E. coli*, while the  $\beta$  subunit is capable of functioning by itself to produce tryptophan from indole, when it is in an  $\alpha\beta$  configuration or in its physiological complex, the allosteric effect enhances the catalytic efficiency. Surprisingly, in contrast to *E. coli*, the LBCA  $\beta$  subunit was found to have a fivefold reduction in the catalytic efficiency when it was found in a complex (32). Although the tryptophan synthase enzyme from the LBCA had the highest homology to the enzyme from *Ct*, the allosteric effect between the two subunits was distinct.

Not surprisingly, when clinical F strains were deprived of tryptophan by IFN- $\gamma$  treatment, they were not able to recover with indole supplementation, similar to ocular strains. When tryptophan was added back to the starved clinical F strains (+IFN- $\gamma$  -Trp +Trp), recoverable IFUs/ml were significantly higher than the tryptophan-starved clinical strains growing in the presence of indole. F/IC-Cal3 had an overall higher growth rate in comparison to the clinical strains, and the addition of indole or tryptophan yielded significantly higher IFUs/ml. These data are supported by the fact that clinical F strains produced significantly smaller inclusions than F/IC-Cal3 under IFN- $\gamma$ -induced tryptophan starvation and indole supplementation (Fig. 6). Furthermore, under the same conditions, the clinical F strains contained many aberrant bodies in the inclusions with few mature infectious elementary bodies (EBs) compared to F/IC-Cal3. These collective data indicate the lack of a functional tryptophan synthase for the clinical F strains.

To assess the ability of clinical F strains to regulate *trpRBA* in a transcriptional manner, mRNA expression levels of *trpBA* were measured during tryptophan starvation with subsequent indole and tryptophan rescue. Consistent with previous work using reference *Ct* strains with and without functional tryptophan operons (25, 46), we found that at 24 hpi during tryptophan starvation, F/IC-Cal3 had significantly higher expression levels of *trpBA* compared with the clinical F strains, indicating that the latter strains cannot upregulate *trpBA* expression and therefore are not capable of synthesizing tryptophan efficiently. This conclusion is supported by our findings that clinical F strain *trpBA* expression levels were relatively similar, regardless of treatment conditions, throughout development at 12, 24, 36, 48, and 60 hpi compared to F/IC-Cal3. Transcription of *trpBA* might also be influenced by additional factors. Recent work has shown that the iron-dependent transcription factor, YtgR, can bind to the intergenic region (IGR) between *trpR* and *trpB*, regulating the expression of the operon (47). Although the clinical F IGR and YtgR transcription factor are similar to those of F/IC-Cal3 (not shown), perhaps additional factors influence the operator near or within the  $\alpha\beta\beta\alpha$  tetramer.

Because *Ct* scavenges host tryptophan pools during tryptophan scarcity, intracellular tryptophan concentration decreases due to competition between the organism and host cell (48). We found that when tryptophan was depleted by IFN- $\gamma$  treatment or tryptophan-depleted media, clinical F strains had higher intracellular tryptophan con-

#### FIG 5 Legend (Continued)

strains F/I-IV, F/IC-Cal3, and A/HAR13 with the PDB templates of LBCA 5ey5, *M. tuberculosis* 5tch, and *S. Typhimurium* 1qopA was performed using Clustal Omega (see Materials and Methods). Residues involved in both catalytic and subunit interaction (magenta),  $\alpha$ -L6 residues  $\alpha$ 176-196 according to the 5tch sequence (cyan), clinical strain F mutation G253D and .254N and .255L aa elongation (yellow), gray, basic amino acids arginine and lysine in template sequences (gray), and acidic amino acid aspartic acid in clinical strains (green) are indicated. (B) Phylogenetic tree of *Ct* strains and PDB aa templates using neighbor joining with Jones-Taylor-Thornton (JTT) substitution method with 10,000 bootstrap replications using MEGA 7 (see Materials and Methods).

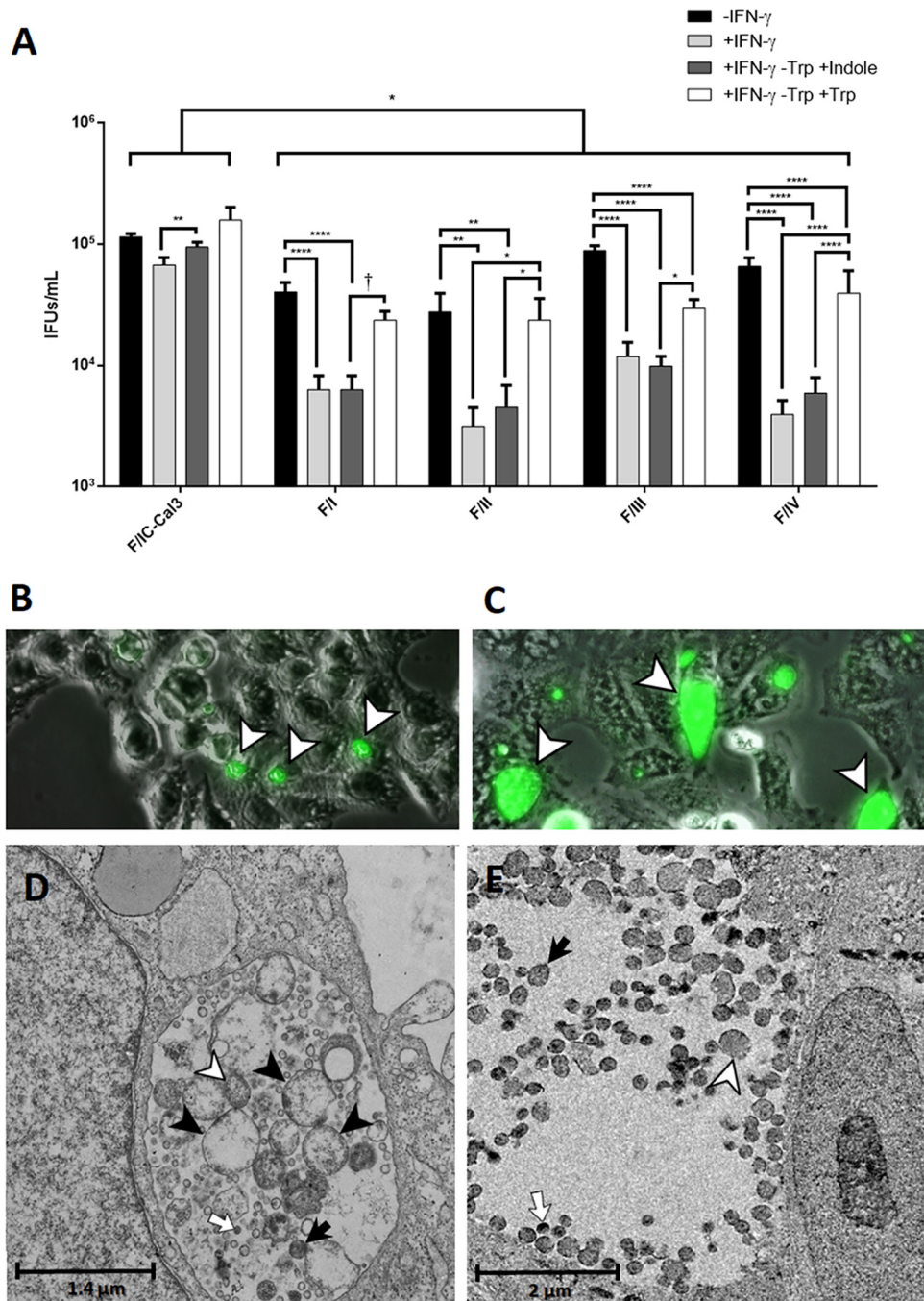


**FIG 6** Recoverable infectivity of *C. trachomatis* clinical strains F I-IV was significantly lower than for F/IC-Cal3 following tryptophan starvation and rescue. Infected cells were incubated for 48 h in the presence of either complete DMEM medium (-IFN- $\gamma$ ), tryptophan-free DMEM medium treated with 5 ng/ml human IFN- $\gamma$  (+IFN- $\gamma$ ), tryptophan-free DMEM medium treated with 5 ng/ml human IFN- $\gamma$  supplemented with 50  $\mu$ M Indole (+IFN- $\gamma$  -Trp +Indole) or 10 mg/liter tryptophan (+IFN- $\gamma$  -Trp +Trp). (A) Comparison between reference strain F/IC-Cal3 and clinical strains F I-IV. Mean recoverable IFUs/ml plus standard deviations (SD) (error bars) from three independent experiments. †,  $P = 0.0597$ ; \*,  $P < 0.05$ ; \*\*,  $P < 0.01$ ; \*\*\*\*,  $P < 0.0001$ . (B) Inclusion morphology of F/IC-Cal3 under IFN- $\gamma$  and indole treatment (+IFN- $\gamma$  -Trp +Indole). Inclusions were stained with a FITC-conjugated Ct-specific LPS MAb (see Materials and Methods). White arrowheads indicate Ct inclusions. (C) Clinical strain F II under IFN- $\gamma$  and indole treatment (+IFN- $\gamma$  -Trp +Indole); inclusions were stained with a Ct-specific LPS-MAb at 48 hpi. The morphology of F I, III, and IV were similar to that of F II (data not shown). Arrowheads indicate Ct inclusions. (D) TEM of clinical strain F II and (E) reference strain F/IC-Cal3 under IFN- $\gamma$  and indole treatment (+IFN- $\gamma$  -Trp +Indole) at 48 hpi. White arrow, Elementary Body; Black arrow, Intermediate Body; white arrowhead, Reticulate Body; black arrowhead, Aberrant Body.

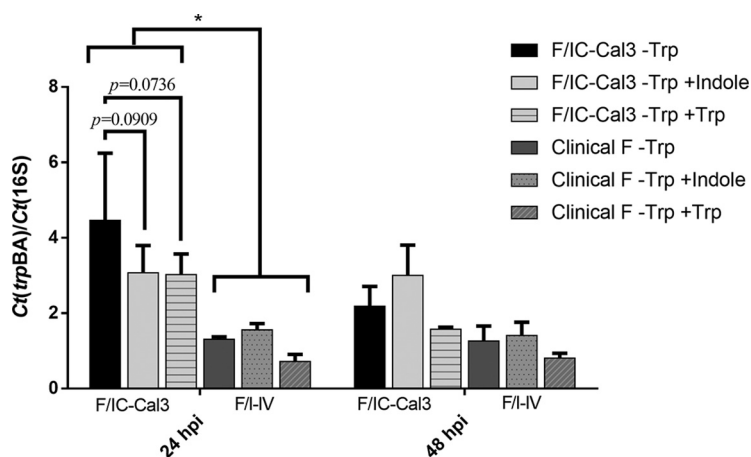


**FIG 7** *trpBA* mRNA expression levels for clinical strains F I-IV were significantly reduced compared to F/IC-Cal3 under tryptophan depletion and rescue. At 48 h before infection, HeLa cells were treated with 5 ng/ml of human IFN- $\gamma$  for 24 h in tryptophan-free media. Infected cells were incubated in the presence of either tryptophan-free DMEM (-Trp), tryptophan-free DMEM supplemented with 100  $\mu$ M indole (-Trp +Indole), or tryptophan-free DMEM supplemented with 10 mg/liter tryptophan (-Trp +Trp). Infected cells were harvested at indicated times. RNA was reversed transcribed to cDNA, and expression levels were normalized to the *Ct* 16S rRNA and presented as means plus SD from three independent experiments. Data are shown for F I, although F II-IV had similar mRNA transcription patterns. There were no statistically significant differences at 48 hpi. \*,  $P < 0.05$ .

centrations compared to F/IC-Cal3, suggesting that F/IC-Cal3 is a stronger competitor at utilizing host tryptophan pools to recover from starvation. When tryptophan-depleted cultures were supplemented with indole, the findings were similar, indicating that F/IC-Cal3 was more efficient at utilizing indole for tryptophan synthesis that in turn was more efficiently metabolized for recovery. These findings were supported by the higher levels of intracellular tryptophan concentrations for the clinical F strains when the cultures were supplemented with tryptophan.

*Ct* is thought to enter a persistent form when tryptophan is depleted by the host immune response, thereby decreasing its metabolic rate to survive (reviewed in reference 49). However, the organism may first scavenge host tryptophan reservoirs to continue its developmental cycle. The risk with the latter scenario is that low tryptophan concentrations in epithelial cells and the surrounding environment may lead to cellular apoptosis (50). Alternatively, entering a persistent state shortly after tryptophan is limited would preserve host cell tryptophan pools as well as provide a protective niche inside the cell for survival. The clinical F strains that we isolated from the same woman resemble the benefits of this *Ct* persistent form during stressful conditions that include repeated antibiotic treatment and nutrient deficiency induced by the host immune response. Resurgence of the infection may have occurred when sufficient tryptophan became available.

*Ct* could have evolved from an ancestor that was initially residing in the gastrointestinal tract (51) where high levels of indole are available. The availability of indole may have also facilitated establishment of the urogenital tract as another tropic site for *Ct* infection. Although the ability to utilize indole is considered an advantage for this obligate intracellular pathogen, perhaps the loss of a functional  $\alpha$  subunit through evolution as for the ocular strains has benefited survival. One part of this may be the energy cost savings in not having to synthesize tryptophan. In any case, it appears that we are now starting to see clinical benefit for this loss of function in sexually transmitted strains.

Although mutations in *trpA* that result in a dysfunctional tryptophan operon were thought to be confined only to ocular strains, the discovery of other mutations among F strains in the present study suggests an additional key evolutionary strategy that allows the organism to survive likely via persistence, even when indole is present. Our

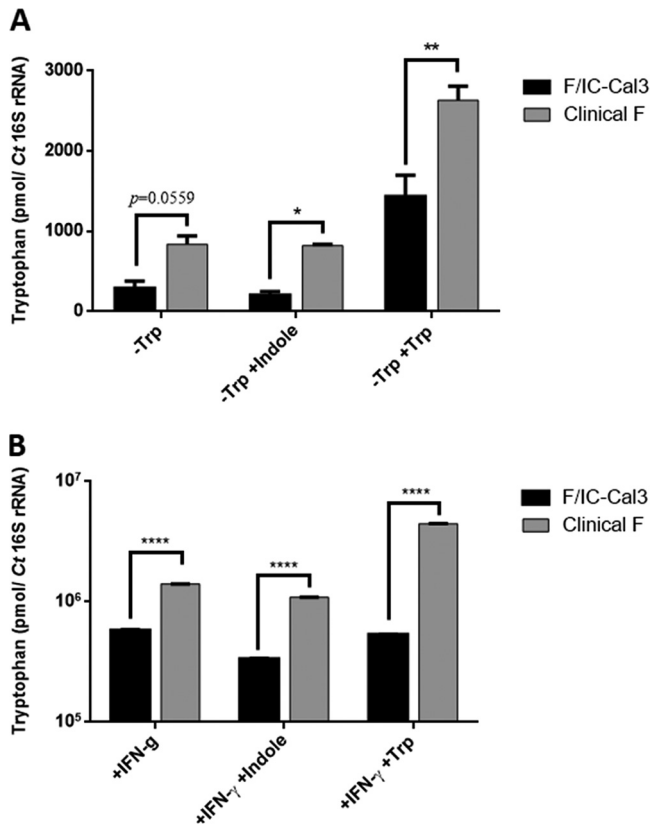


**FIG 8** *In vitro* intracellular tryptophan concentrations vary significantly for reference strain F/IC-Cal3 compared with clinical strains F I-IV. (A and B) *Ct*-infected HeLa cells were incubated with either tryptophan-free DMEM medium (–Trp) (A) or complete medium treated with IFN- $\gamma$  (+IFN- $\gamma$ ) (B) (see Materials and Methods). The medium was supplemented with indole (–Trp +Indole or +IFN- $\gamma$  +Indole) or tryptophan (–Trp +Trp or +IFN- $\gamma$  +Trp) as indicated. Infected cells were harvested at 48 hpi, and intracellular tryptophan concentrations were measured using high-pressure liquid chromatography-linked tandem mass spectrometry (see Materials and Methods). Data are presented as the mean tryptophan concentration (in picomoles) normalized to *Ct* 16S rRNA plus SD based on two independent experiments. \*,  $P < 0.05$ ; \*\*,  $P < 0.01$ ; \*\*\*\*,  $P < 0.0001$ .

data indicate that these mutations affected the structure of the  $\alpha\beta\beta\alpha$  tetramer and, thereby, impact the regulation and function of the operon for the synthesis of tryptophan from indole. Furthermore, this study supports the notion that, during IFN- $\gamma$ -induced IDO activity and depletion of tryptophan, clinical urogenital *Ct* strains can develop persistent infections *in vivo*. These strains may periodically be able to cause an active infection when tryptophan becomes available, perhaps explaining the recurrence of infections over many years for the patient in our study.

## MATERIALS AND METHODS

### Sample collection, *C. trachomatis* clinical strain isolation, and whole-genome sequencing.

Endocervical flock swabs (Copan, Murrieta, CA) were collected from women attending health clinics in the San Francisco Bay Area as part of a larger study and were supplied deidentified with no trace to the patient's name. Hence, the institutional review board (IRB) at University of California San Francisco Benioff Children's Hospital Oakland determined that this research does not involve human subjects.

Swab samples were placed in cryovials containing 1 ml of M4 medium (Thermo-Fisher, Waltham, MA) and kept at  $-80^{\circ}\text{C}$  until processed. *C. trachomatis* (*Ct*) was isolated from a female with four chronological ( $>4$  years) STIs who had been treated with doxycycline or azithromycin for each documented infection. *Ct* was isolated as previously described (52). Briefly, at 48 hpi, infected cells were harvested, propagated, and purified by density gradient centrifugation as previously described (52). Genomic DNA was purified from each isolate, termed F I, F II, F III, and F IV, with subsequent whole-genome sequencing as we described previously (29). *ompA* and *trpRBA* were resequenced for verification as described previously (52). Table S1 in the supplemental material lists the primers used in this study.

**Phylogeny of *C. trachomatis* clinical strains F I-IV *trpRBA* and *TrpRBA*.** *trpRBA* and *TrpRBA* sequences from the four isolates F I to IV (F I-IV) were compared for nucleotide (nt) and amino acid (aa)

differences using MEGA 7 (<https://mafft.cbrc.jp/alignment/software/>). Sequences from seven San Francisco Bay Area clinical F strains and 59 F strains from all public databases were aligned with F I-IV and 20 Ct reference strains (Fig. 1, Fig. 2). Maximum likelihood trees were constructed as previously described (29) with 10,000 bootstrap replicates. For aa phylogenies, maximum likelihood trees were constructed using Jones-Taylor-Thornton (JTT) substitution model with 500 bootstrap replicates. Ct TrpA and TrpB were also aligned with homologs from other organisms using neighbor joining to detect significant subfamily conserved residues that may be evolutionarily related (29).

**Comparative TrpA and TrpB structure analyses of *C. trachomatis* clinical and reference strains with homologous species.** F I-IV, F/IC-Cal3, and A/HAR13 TrpA and TrpB sequences were uploaded to MODBASE (<http://salilab.org/modbase>), and comparative protein three-dimensional modeling structures were calculated using MODELLER (53) with pairwise sequence alignment, sequence-sequence, sequence-profile, and PSI-BLAST methods (54). CHIMERA was used for structural visualization (55). Protein structures were analyzed by satisfaction of spatial restraint (56). The reconstructed putative LBCA tryptophan synthase 5ey5 had the highest homology to Ct  $\alpha$  and  $\beta$  subunits, followed by *M. tuberculosis* 5tch and *S. Typhimurium* 1qop. Ct sequences were aligned with 5ey5, 5tch, and 1qop using Multalign-Viewer extension (57) and Clustal Omega (58). Ct TrpA models were then generated based on the 5ey5 protein structure (homology score of 32.16% to F I-IV, 34.43% [based on 183 aa] to A/HAR13 and 32.02% to F/IC-Cal3). Ct TrpB models were similarly based on 5ey5 with 56.12% homology to F I-IV and F/IC-Cal3 and 55.87% to A/HAR13.

To authenticate MODELLER structure and functional residue predictions, TrpA domain architectures were determined using Conserved Domain (CD) (59), Protein family (Pfam) (60), Simple Modular Architecture Research Tool (SMART) (61), Transmembrane helix prediction (TMHMM) (62), and SignalP (63) tools. Protein BLAST (64) against the Protein Data Bank (PDB) using a 0.01 cutoff E value and Protein Homology/analogy Recognition Engine (Phyre) (65) were performed to obtain additional homologs that could represent the F I-IV TrpA structure.

Ct putative active ligand-binding sites, the indole tunnel, TrpA-TrpB communication (COMM) domain, and nonsynonymous mutations were manually identified and visualized on the predicted models, based on previous work and crystal structures of different *Escherichia coli* and *S. Typhimurium* mutants (24, 43–45, 66–68).

***C. trachomatis* in vitro tryptophan starvation and rescue assays.** HeLa229 cell monolayers were inoculated with F I-IV or F/IC-Cal3 at a multiplicity of infection (MOI) of 3. For recoverable infectivity assays, inoculates were incubated in either complete Dulbecco modified Eagle medium (DMEM) (Thermo-Fisher) (–IFN- $\gamma$ ), tryptophan-free DMEM treated with 5 ng/ml human IFN- $\gamma$  (+IFN- $\gamma$ ) (Sigma-Aldrich), tryptophan-free DMEM with 5 ng/ml human IFN- $\gamma$  supplemented with 50  $\mu$ M indole (+IFN- $\gamma$  –Trp +Indole) (Sigma-Aldrich), or 10 mg/liter tryptophan (+IFN- $\gamma$  –Trp +Trp). For *trpBA* mRNA transcription assays, inoculates were incubated in either tryptophan-free DMEM (–Trp), tryptophan-free DMEM supplemented with 100  $\mu$ M indole (–Trp +Indole) or tryptophan-free DMEM supplemented with 10 mg/liter tryptophan (–Trp +Trp). For intracellular tryptophan concentrations, inoculates were incubated in tryptophan-free DMEM, DMEM supplemented with 100  $\mu$ M indole, DMEM supplemented with 10 mg/liter tryptophan, or with complete CMGH medium supplemented with IFN- $\gamma$  alone (+IFN- $\gamma$ ), IFN- $\gamma$  and indole (+IFN- $\gamma$  +Indole), or IFN- $\gamma$  and tryptophan (+IFN- $\gamma$  +Trp). Cultures were incubated for 24 or 48 h (37°C, 5% CO<sub>2</sub>) as indicated.

**Recoverable infectious progeny of *C. trachomatis* clinical strains F I-IV compared to reference strain F/IC-Cal3 following tryptophan starvation and rescue.** The initial infected cultures were used to infect fresh HeLa cell monolayers, incubated for 44 to 48 h, fixed with methanol, and stained using fluorescein isothiocyanate (FITC)-conjugated Ct-specific lipopolysaccharide (LPS) monoclonal antibody (Mab) (Virostat, Westbrook, ME) and Hoechst (to detect nuclei) for enumerating inclusion-forming units per milliliter (IFUs/ml) as we described previously (69).

**Microscopy and transmission electron microscopy.** Morphological characteristics in cell culture were evaluated with fluorescence and transmission electron microscopy (TEM) over the course of *in vitro* development. At 48 hpi, coverslips were fixed and stained, and IFUs/ml were enumerated as described above. Imaris X64 software was used to calculate inclusion area as square micrometers as we described previously (69).

Infected cultures were harvested for TEM characterization as we described previously (69). Briefly, wells were washed with phosphate-buffered saline (PBS) (Mediatech, Herndon, VA) containing 2% glutaraldehyde in 0.1 M sodium cacodylate (Electron Microscope Lab [EML] at University of California [UC] Berkeley), pelleted at 200  $\times$  g, and prefixed in 2% glutaraldehyde in 0.1 M sodium cacodylate. The samples were refrigerated at 4°C for 24 h prior to postfixation with 1% osmium tetroxide in 0.1 M sodium cacodylate and washed in 0.1 M sodium cacodylate buffer and 0.5% aqueous uranyl acetate overnight. Cells were dehydrated using a graduated ethanol series, embedded in Epon-Araldite resin, and allowed to polymerize. A Riechert Ultracut MT6000 microtome was used to slice 60- to 90-nm sections prior to staining with 2% uranyl acetate and Reynolds lead citrate. A Tecnai 12 TEM (EML) was used for imaging.

**mRNA expression of *trpR* and *trpBA* following tryptophan starvation and rescue.** By using an MOI of 3, 100% of the cells were infected. Infected cells were incubated as described above and harvested at 24 and 48 hpi (69). Briefly, total RNA was extracted and reverse transcribed to cDNA and subjected to quantitative reverse transcription-PCR (qRT-PCR) with two replicates of each cDNA sample and control. 16S rRNA gene expression was used as a control for the number of Ct organisms; the human  $\beta$ -actin gene was used as a control for host cell viability. Normalization of the 16S rRNA gene to  $\beta$ -actin gene was used for relative Ct growth.

**Intracellular tryptophan concentrations.** At 48 hpi, infected cells were pelleted and resuspended in perchloric acid (Sigma-Aldrich) (10% wt/vol) solution containing 1 mM diethylenetriamine pentaacetate (Sigma-Aldrich) for cell lysis, followed by 4°C centrifugation at 1,500 rpm. Tryptophan concentrations were measured in supernatants using high-performance liquid chromatography-linked tandem mass spectrometry (HPLC-MS/MS) with the EZ-FAAST aa derivatization kit (Phenomenex, Torrance, CA) as previously described (70). Briefly, supernatants containing tryptophan were mixed with an internal standard (tyrosine 3,3-D<sub>2</sub>), and pellets were mixed with a strong cation exchange resin (Phenomenex, Torrance, CA). Derivatization was performed using the manufacturer's protocols. Derivative products were extracted with isoctane (Sigma-Aldrich), dried under nitrogen, and reconstituted with a mobile phase. Analytes were quantified based on purified standard compounds. Data were normalized against Ct 16S rRNA gene transcription levels.

**Statistical analysis.** Data were analyzed using Prism GraphPad V.6. Statistical significance was determined using two-way analysis of variance (ANOVA); *P* values were calculated using Tukey's multiple-comparison test. A *P* value of <0.05 was considered significant.

## SUPPLEMENTAL MATERIAL

Supplemental material for this article may be found at <https://doi.org/10.1128/mBio.01464-19>.

**FIG S1**, TIF file, 1.1 MB.

**TABLE S1**, DOCX file, 0.01 MB.

## ACKNOWLEDGMENTS

We thank Elaine Meng for her help with the MODELLER and Chimera software and Derek Wan for compiling the *trpRBA* sequences from the SRA database.

This work was supported by NIH Public Health Service grants R01AI098843 and R01AI059647 (D.D.).

## REFERENCES

- World Health Organization. 2016. Sexually transmitted infections (STIs), fact sheet. World Health Organization, Geneva, Switzerland.
- van Liere GA, Dukers-Muijers NH, Levels L, Hoebbe CJ. 2017. High proportion of anorectal *Chlamydia trachomatis* and *Neisseria gonorrhoeae* after routine universal urogenital and anorectal screening in women visiting the STI clinic. *Clin Infect Dis* 12:1705–1710. <https://doi.org/10.1093/cid/cix243>.
- Newman L, Rowley J, Vander Hoorn S, Wijesooriya NS, Unemo M, Low N, Stevens G, Gottlieb S, Kiarie J, Temmerman M. 2015. Global estimates of the prevalence and incidence of four curable sexually transmitted infections in 2012 based on systematic review and global reporting. *PLoS One* 10:e0143304. <https://doi.org/10.1371/journal.pone.0143304>.
- Darville T, Thomas HJ. 2010. Pathogenesis of genital tract disease due to *Chlamydia trachomatis*. *J Infect Dis* 201:S114–S125. <https://doi.org/10.1086/652397>.
- Dean D. 2010. Pathogenesis of chlamydial ocular infections, p 678–702. In Tasman W, Jaeger E (ed), *Duane's foundations of clinical ophthalmology*. Lippincott Williams & Wilkins, Philadelphia, PA.
- Last AR, Pickering H, Roberts CH, Coll F, Phelan J, Burr SE, Cassama E, Nabicassa M, Seth-Smith HMB, Hadfield J, Cutcliffe LT, Clarke IN, Mabey DCW, Bailey RL, Clark TG, Thomson NG, Holland MJ. 2018. Population-based analysis of ocular *Chlamydia trachomatis* in trachoma-endemic West African communities identifies genomic markers of disease severity. *Genome Med* 10:15. <https://doi.org/10.1186/s13073-018-0521-x>.
- Dean D, Suchland RJ, Stamm WE. 2000. Evidence for long-term cervical persistence of *Chlamydia trachomatis* by omp1 genotyping. *J Infect Dis* 182:909–916. <https://doi.org/10.1086/315778>.
- Lars W, Riduan J, Gladys R, Hagdu A, Thompson S. 1992. Pelvic inflammatory disease and fertility: a cohort study of 1844 women with laparoscopically verified disease and 657 control women with normal laparoscopic results. *Sex Transm Dis* 19:185–192.
- Meijer C, Weiderpass E, Arslan A, Posso H, Franceschi S, Ronderos M, Mun N, Van Den Brule AJC. 2005. The natural course of *Chlamydia trachomatis* infection in asymptomatic Colombian women: a 5-year follow-up study. *J Infect Dis* 191:907–916. <https://doi.org/10.1086/428287>.
- Geisler WM. 2007. Management of uncomplicated *Chlamydia trachomatis* infections in adolescents and adults: evidence reviewed for the 2006 Centers for Disease Control and Prevention sexually transmitted diseases treatment guidelines. *Clin Infect Dis* 44:S77–S83. <https://doi.org/10.1086/511421>.
- Owusu-Edusei K, Gift TL, Chesson HW, Kent CK. 2013. Practice of epidemiology investigating the potential public health benefit of jail-based screening and treatment programs for *Chlamydia*. *Am J Epidemiol* 177:463–473. <https://doi.org/10.1093/aje/kws240>.
- Brunham RC, Pourbohloul B, Mak S, White R, Rekart ML. 2005. The unexpected impact of a *Chlamydia trachomatis* infection control program on susceptibility to reinfection. *J Infect Dis* 192:1836–1844. <https://doi.org/10.1086/497341>.
- Atik B, Thanh TT, Luong VQ, Lagree S, Dean D. 2006. Impact of annual targeted treatment on infectious trachoma and susceptibility to reinfection. *JAMA* 296:1488–1497. <https://doi.org/10.1001/jama.296.12.1488>.
- Perry LL, Su H, Feilzer K, Messer R, Hughes S, Whitmire W, Caldwell HD. 1999. Differential sensitivity of distinct *Chlamydia trachomatis* isolates to IFN-gamma-mediated inhibition. *J Immunol* 162:3541–3548.
- Brunham RC, Rekart ML. 2008. The arrested immunity hypothesis and the epidemiology of *Chlamydia* control. *Sex Transm Dis* 35:53–54. <https://doi.org/10.1097/OLQ.0b013e31815e41a3>.
- Ong VA, Marsh JW, Lawrence A, Allan JA, Timms P, Huston WM. 2013. The protease inhibitor JO146 demonstrates a critical role for CtHtrA for *Chlamydia trachomatis* reversion from penicillin persistence. *Front Cell Infect Microbiol* 3:100. <https://doi.org/10.3389/fcimb.2013.00100>.
- Dreeses-Werringloer U, Padubrin I, Zeidler H, Köhler L. 2001. Effects of azithromycin and rifampin on *Chlamydia trachomatis* infection in vitro. *Antimicrob Agents Chemother* 45:3001–3008. <https://doi.org/10.1128/AAC.45.11.3001-3008.2001>.
- Last AR, Burr SE, Harding-Esch E, Cassama E, Nabicassa M, Roberts C, Mabey DCW, Holland MJ, Bailey RL. 2017. The impact of a single round of community mass treatment with azithromycin on disease severity and ocular *Chlamydia trachomatis* load in treatment-naïve trachoma-endemic island communities in West Africa. *Parasit Vectors* 10:624. <https://doi.org/10.1186/s13071-017-2566-x>.
- West SK, Moncada J, Munoz B, Mkocho H, Storey P, Hardick J, Gaydos CA, Quinn TC, Schachter J. 2014. Is there evidence for resistance of ocular *Chlamydia trachomatis* to azithromycin after mass treatment for trachoma control? *J Infect Dis* 210:65–71. <https://doi.org/10.1093/infdis/jiu046>.
- Bhengraj AR, Vardhan H, Srivastava P, Salhan S, Mittal A. 2010. Decreased susceptibility to azithromycin and doxycycline in clinical isolates of *Chlamydia trachomatis* obtained from recurrently infected

- female patients in India. *Chemotherapy* 56:371–377. <https://doi.org/10.1159/000314998>.
21. McClarty G. 1994. *Chlamydiae* and the biochemistry of intracellular parasitism. *Trends Microbiol* 2:157–164. [https://doi.org/10.1016/0966-842X\(94\)90665-3](https://doi.org/10.1016/0966-842X(94)90665-3).
  22. Beatty WL, Morrison RP, Byrne GI. 1994. Persistent *Chlamydiae*: from cell culture to a paradigm for chlamydial pathogenesis. *Microbiol Rev* 58: 686–699.
  23. Belland RJ, Nelson DE, Virok D, Crane DD, Hogan D, Sturdevant D, Beatty WL, Caldwell HD. 2003. Transcriptome analysis of chlamydial growth during IFN-gamma-mediated persistence and reactivation. *Proc Natl Acad Sci U S A* 100:15971–15976. <https://doi.org/10.1073/pnas.2535394100>.
  24. Fehner-Gardiner C, Roshick C, Carlson JH, Hughes S, Belland RJ, Caldwell HD, McClarty G. 2002. Molecular basis defining human *Chlamydia trachomatis* tissue tropism. A possible role for tryptophan synthase. *J Biol Chem* 277:26893–26903. <https://doi.org/10.1074/jbc.M203937200>.
  25. Caldwell HD, Wood H, Crane D, Bailey R, Jones RB, Mabey D, Maclean I, Mohammed Z, Peeling R, Roshick C, Schachter J, Solomon AW, Stamm WE, Suchland RJ, Taylor L, West SK, Quinn TC, Belland RJ, McClarty G. 2003. Polymorphisms in *Chlamydia trachomatis* tryptophan synthase genes differentiate between genital and ocular isolates. *J Clin Invest* 111:1757–1769. <https://doi.org/10.1172/JCI17993>.
  26. Merkl R. 2007. Modelling the evolution of the archeal tryptophan synthase. *BMC Evol Biol* 20:1–20. <https://doi.org/10.1186/1471-2148-7-59>.
  27. Ziklo N, Huston WM, Hocking JS, Timms P. 2016. *Chlamydia trachomatis* genital tract infections: when host immune response and the microbiome collide. *Trends Microbiol* 24:750–765. <https://doi.org/10.1016/j.tim.2016.05.007>.
  28. Ziklo N, Huston WM, Taing K, Katouli M, Timms P. 2016. *In vitro* rescue of genital strains of *Chlamydia trachomatis* from interferon- $\gamma$  and tryptophan depletion with indole-positive, but not indole-negative *Prevotella spp.* *BMC Microbiol* 16:286. <https://doi.org/10.1186/s12866-016-0903-4>.
  29. Joseph SJ, Didelot X, Rothschild J, Vries HJC, De Morre SA, Read TD, Dean D. 2012. Population genomics of *Chlamydia trachomatis*: insights on drift, selection, recombination, and population structure. *Mol Biol Evol* 29:3933–3946. <https://doi.org/10.1093/molbev/mss198>.
  30. Eswar N, Webb B, Marti-Renom MA, Madhusudhan MS, Eramian D, Shen M, Pieper U, Sali A. 2006. Comparative protein structure modeling using Modeller. *Curr Protoc Bioinformatics Chapter 5:Unit-5.6*. <https://doi.org/10.1002/0471250953.bi0506s15>.
  31. Eswar N, John B, Mirkovic N, Fiser A, Ilyin VA, Pieper U, Stuart AC, Marti-Renom MA, Madhusudhan MS, Yerkovich B, Sali A. 2003. Tools for comparative protein structure modeling and analysis. *Nucleic Acids Res* 31:3375–3380. <https://doi.org/10.1093/nar/gkg543>.
  32. Busch F, Rajendran C, Heyn K, Schlee S, Merkl R, Sterner R. 2016. Ancestral tryptophan synthase reveals functional sophistication of primordial enzyme complexes. *Cell Chem Biol* 23:709–715. <https://doi.org/10.1016/j.chembiol.2016.05.009>.
  33. Ngo H, Kimmich N, Harris R, Niks D, Blumenstein L, Kulik V, Barends TR, Schlichting I, Dunn MF. 2007. Allosteric regulation of substrate channeling in tryptophan synthase: modulation of the L-serine reaction in stage I of the beta-reaction by alpha-site ligands. *Biochemistry* 46:7740–7753. <https://doi.org/10.1021/bi7003872>.
  34. Read TD, Brunham RC, Shen C, Gill SR, Heidelberg JF, White O, Hickey EK, Peterson J, Utterback T, Berry K, Bass S, Linher K, Weidman J, Khouri H, Craven B, Bowman C, Dodson R, Gwinn M, Nelson W, DeBoy R, Kolonay J, McClarty G, Salzberg SL, Eisen J, Fraser CM. 2000. Genome sequences of *Chlamydia trachomatis* MoPn and *Chlamydia pneumoniae* AR39. *Nucleic Acids Res* 28:1397–1406. <https://doi.org/10.1093/nar/28.6.1397>.
  35. Dong Q, Brulic JM, Iovieno A, Bates B, Garoutte A, Miller D, Revanna KV, Gao X, Antonopoulos DA, Slepak VZ, Shestopalov VI. 2011. Diversity of bacteria at healthy human conjunctiva. *Invest Ophthalmol Vis Sci* 52: 5408–5413. <https://doi.org/10.1167/iovs.10-6939>.
  36. Aiyar A, Quayle AJ, Buckner LR, Sherchand SP, Chang TL, Zea AH, Martin DH, Belland RJ. 2014. Influence of the tryptophan-indole-IFN $\gamma$  axis on human genital *Chlamydia trachomatis* infection: role of vaginal co-infections. *Front Cell Infect Microbiol* 4:72. <https://doi.org/10.3389/fcimb.2014.00072>.
  37. Willcox MDP. 2013. Characterization of the normal microbiota of the ocular surface. *Exp Eye Res* 117:99–105. <https://doi.org/10.1016/j.exer.2013.06.003>.
  38. Ooz C, July R. 1971. The B protein of *Escherichia coli* tryptophan synthase, new beta-elimination and beta-replacement reactions. *Biochem Biophys Res Commun* 44:1271–1278.
  39. Suzuki H, Yanaka A, Shibahara T, Matsui H, Nakahara A, Tanaka N, Muto H, Momoi T, Uchiyama Y. 2002. Ammonia-induced apoptosis is accelerated at higher pH in gastric surface mucous cells. *Am J Physiol Gastrointest Liver Physiol* 283:G986–G995. <https://doi.org/10.1152/ajpgi.00482.2001>.
  40. Iyer G, Agarwal S, Srinivasan B, Narayanasamy A. 2018. Isolation of acid from eye drop bottles being used by patients presenting with presumed scleritis. *Indian J Ophthalmol* 66:1084–1087. [https://doi.org/10.4103/ijoo.IJO\\_82\\_18](https://doi.org/10.4103/ijoo.IJO_82_18).
  41. Sherchand SP, Aiyar A. 2019. Ammonia generation by tryptophan synthase drives a key genetic difference between genital and ocular *Chlamydia trachomatis* isolates. *Proc Natl Acad Sci U S A* <https://doi.org/10.1073/pnas.1821652116>.
  42. Yanofsky C, Horn V. 1972. Tryptophan synthetase chain positions affected by mutations near the ends of the genetic map of *trpA* of *Escherichia coli*. *J Biol Chem* 247:4494–4499.
  43. Brzovic PS, Sawa Y, Hyde CC, Miles EW, Dunn MF. 1992. Evidence that mutations in a loop region of the alpha-subunit inhibit the transition from an open to a closed conformation in the tryptophan synthase holoenzyme complex. *J Biol Chem* 267:13028–13038.
  44. Hyde CC, Ahmed SA, Padlan EA, Miles EW, Davies DR. 1988. Three-dimensional structure of the tryptophan synthase  $\alpha_2\beta_2$  multienzyme complex from *Salmonella typhimurium*. *J Biol Chem* 263:17857–17871.
  45. Raboni S, Bettati S, Mozzarelli A. 2005. Identification of the geometric requirements for allosteric communication between the alpha and beta subunits of tryptophan synthase. *J Biol Chem* 280:13450–13456. <https://doi.org/10.1074/jbc.M414521200>.
  46. Wood H, Fehner-Gardner C, Berry J, Fischer E, Graham B, Hackstadt T, Roshick C, McClarty G. 2003. Regulation of tryptophan synthase gene expression in *Chlamydia trachomatis*. *Mol Microbiol* 49:1347–1359. <https://doi.org/10.1046/j.1365-2958.2003.03638.x>.
  47. Pokorzynski ND, Brinkworth AJ, Carabeo RA. 2018. The iron-dependent repressor YtgR regulates the tryptophan salvage pathway through a bipartite mechanism of transcriptional control in *Chlamydia trachomatis*. [bioRxiv https://doi.org/10.1101/322586](https://doi.org/10.1101/322586).
  48. Kane CD, Vena RM, Ouellette SP, Byrne GI. 1999. Intracellular tryptophan pool sizes may account for differences in gamma interferon-mediated inhibition and persistence of chlamydial growth in polarized and non-polarized cells. *Infect Immun* 67:1666–1671.
  49. Panzetta ME, Valdivia RH, Saka HA. 2018. *Chlamydia* persistence: a survival strategy to evade antimicrobial effects *in-vitro* and *in-vivo*. *Front Microbiol* 9:3101. <https://doi.org/10.3389/fmicb.2018.03101>.
  50. Oh JE, Shim KY, Lee JI, Choi SI, Baik SK, Eom YW. 2017. 1-Methyl-L-tryptophan promotes the apoptosis of hepatic stellate cells arrested by interferon- $\gamma$  by increasing the expression of IFN- $\gamma$ R $\beta$ , IRF-1 and FAS. *Int J Mol Med* 40:576–582. <https://doi.org/10.3892/ijmm.2017.3043>.
  51. Rank RG, Yeruva L. 2014. Hidden in plain sight: chlamydial gastrointestinal infection and its relevance to persistence in human genital infection. *Infect Immun* 82:1362–1371. <https://doi.org/10.1128/IAI.01244-13>.
  52. Somboonna N, Mead S, Liu J, Dean D. 2008. Discovering and differentiating new and emerging clonal populations of *Chlamydia trachomatis* with a novel shotgun cell culture harvest assay. *Emerg Infect Dis* 14: 445–453. <https://doi.org/10.3201/eid1403.071071>.
  53. Pieper U, Eswar N, Braberg H, Madhusudhan MS, Davis FP, Stuart AC, Mirkovic N, Rossi A, Marti-Renom MA, Fiser A, Webb B, Greenblatt D, Huang CC, Ferrin TE, Sali A. 2004. MODBASE, a database of annotated comparative protein structure models, and associated resources. *Nucleic Acids Res* 32:D217–D222. <https://doi.org/10.1093/nar/gkh095>.
  54. Altschul SF, Madden TL, Schäffer AA, Zhang J, Zhang Z, Miller W, Lipman DJ. 1997. Gapped BLAST and PSI-BLAST: a new generation of protein database search programs. *Nucleic Acids Res* 25:3389–3402. <https://doi.org/10.1093/nar/25.17.3389>.
  55. Meng EC, Pettersen EF, Couch GS, Huang CC, Ferrin TE. 2006. Tools for integrated sequence-structure analysis with UCSF Chimera. *BMC Bioinformatics* 7:1–10. <https://doi.org/10.1186/1471-2105-7-339>.
  56. Sali A, Blundell TL. 1993. Comparative protein modelling by satisfaction of spatial restraints. *J Mol Biol* 234:779–815. <https://doi.org/10.1006/jmbi.1993.1626>.
  57. Pettersen EF, Goddard TD, Huang CC, Couch GS, Greenblatt DM, Meng EC, Ferrin TE. 2004. UCSF chimera — a visualization system for exploratory research and analysis. *J Comput Chem* 25:1605–1612. <https://doi.org/10.1002/jcc.20084>.

58. Sievers F, Wilm A, Dineen D, Gibson TJ, Karplus K, Li W, Lopez R, McWilliam H, Remmert M, Soding J, Thompson JD, Higgins DG. 2011. Fast, scalable generation of high-quality protein multiple sequence alignments using Clustal Omega. *Mol Syst Biol* 7:539. <https://doi.org/10.1038/msb.2011.75>.
59. Marchler-Bauer A, Bo Y, Han L, He J, Lanczycki CJ, Lu S, Chitsaz F, Derbyshire MK, Geer RC, Gonzales NR, Gwadz M, Hurwitz DI, Lu F, Marchler GH, Song JS, Thanki N, Wang Z, Yamashita RA, Zhang D, Zheng C, Geer LY, Bryant SH. 2017. CDD/SPARCLE: functional classification of proteins via subfamily domain architectures. *Nucleic Acids Res* 45:D200–D203. <https://doi.org/10.1093/nar/gkw1129>.
60. El-Gebali S, Mistry J, Bateman A, Eddy SR, Potter SC, Qureshi M, Richardson LJ, Salazar GA, Smart A, Sonnhammer ELL, Hirsh L, Paladin L, Piovesan D, Tosatto SCE, Finn RD. 2019. The Pfam protein families database in 2019. *Nucleic Acids Res* 47:D427–D432. <https://doi.org/10.1093/nar/gky995>.
61. Letunic I, Bork P. 2018. 20 years of the SMART protein domain annotation. *Nucleic Acids Res* 46:D493–D496. <https://doi.org/10.1093/nar/gkx922>.
62. Krogh A, Larsson B, von Heijne G, Sonnhammer ELL. 2001. Predicting transmembrane protein topology with a hidden Markov model: application to complete genomes. *J Mol Biol* 305:567–580. <https://doi.org/10.1006/jmbi.2000.4315>.
63. Petersen TN, Brunak S, von Heijne G, Nielsen H. 2011. SignalP 4.0: discriminating signal peptides from transmembrane regions. *Nat Meth* 8:785–786. <https://doi.org/10.1038/nmeth.1701>.
64. Altschul SF, Wootton JC, Gertz EM, Agarwala R, Morgulis A, Schäffer AA, Yu Y-K. 2005. Protein database searches using compositionally adjusted substitution matrices. *FEBS J* 272:5101–5109. <https://doi.org/10.1111/j.1742-4658.2005.04945.x>.
65. Kelley LA, Mezulis S, Yates CM, Wass MN, Sternberg M. 2015. The Phyre2 web portal for protein modelling, prediction and analysis. *Nat Protoc* 10:845–858. <https://doi.org/10.1038/nprot.2015.053>.
66. Nichols BP, Yanofsky C. 1979. Nucleotide sequences of *trpA* of *Salmonella typhimurium* and *Escherichia coli*: an evolutionary comparison. *Proc Natl Acad Sci U S A* 76:5244–5248. <https://doi.org/10.1073/pnas.76.10.5244>.
67. Hilario E, Caulkins BG, Huang YM, You W, Chang CA, Mueller LJ, Dunn MF, Fan L. 2016. Visualizing the tunnel in tryptophan synthase with crystallography: insights into a selective filter for accommodating indole and rejecting water. *Biochim Biophys Acta* 1864:268–279. <https://doi.org/10.1016/j.bbapap.2015.12.006>.
68. Buller AR, Brinkmann-Chen S, Romney DK, Herger M, Murciano-Calles J, Arnold FH. 2015. Directed evolution of the tryptophan synthase  $\beta$ -subunit for stand-alone function recapitulates allosteric activation. *Proc Natl Acad Sci U S A* 112:14599–14604. <https://doi.org/10.1073/pnas.1516401112>.
69. Recuero-Checa MA, Sharma M, Lau C, Watkins PA, Gaydos CA, Dean D. 2016. *Chlamydia trachomatis* growth and development requires the activity of host long-chain acyl-CoA synthetases (ACSLs). *Sci Rep* 6:1–15. <https://doi.org/10.1038/srep23148>.
70. Morris CR, Suh JH, Hagar W, Larkin S, Bland DA, Steinberg MH, Vichinsky EP, Shigenaga M, Ames B, Kuypers FA, Klings ES. 2008. Erythrocyte glutamine depletion, altered redox environment, and pulmonary hypertension in sickle cell disease. *Blood* 111:402–411. <https://doi.org/10.1182/blood-2007-04-081703>.